Design, fabrication and validation of an ankle-foot orthosis simulator system to optimize mechanical characteristics of AFOs for humans with impaired locomotion

Master's Thesis Lars Wouterse

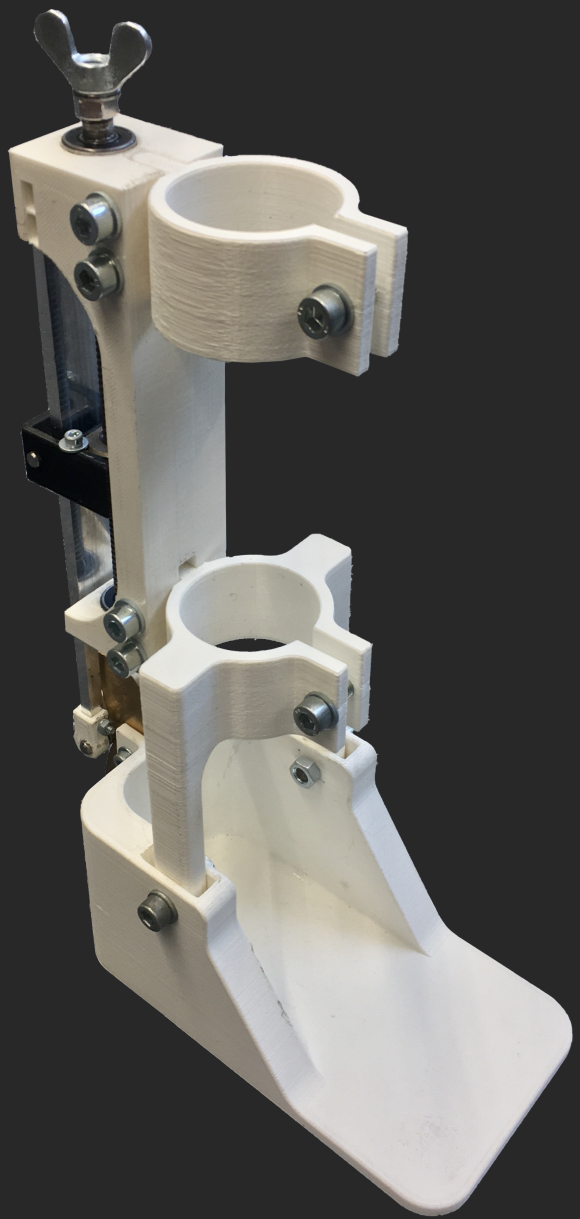

Design, fabrication and validation of an ankle-foot orthosis simulator system to optimize mechanical characteristics of AFOs for humans with impaired locomotion

by

Lars Wouterse

to obtain the degree of Master of Science
at the Delft University of Technology,
to be defended publicly on Thursday August 27, 2020 at 08:30 AM.

Student number:	4304128	
Project duration:	January 1, 2020 – August 27, 2020	
Thesis committee:	Prof. dr. ir. Jaar Harlaar,	TU Delft, supervisor
	Dr. ir. Gerwin Smit,	TU Delft, supervisor
	Prof. dr. ir. Paul Breedveld,	TU Delft

An electronic version of this thesis is available at `http://repository.tudelft.nl/`.

Acknowledgements

First of all, I would like to thank Jaap Harlaar for giving me the opportunity to work on this exciting project, for his guidance and connecting me with the right people. I would like to thank Gerwin Smit, Ajay Seth and Erin Macri for their useful feedback, creative input and critical questions during video calls and lab meetings. Also, Niels Waterval for his feedback and expertise and for enabling me to test the design at the VUmc, and Yvette Kerkum and Peter de Groot of OIM Orthopedie who helped me with their feedback and practical knowledge in the field of assistive devices.

Furthermore, I greatly appreciate the practical knowledge and feedback provided by Cor Meijneke at the start of the project and Jan van Frankenhuyzen at the end of the project. Without Jan I would not have been able to have had such a smooth fabrication and assembly of the design. Finally, I would like to thank Nikko van Crey of the Neurobionics lab at the University of Michigan for his input and feedback.

Acronyms

BRUCE Bi-articular Reciprocal Universal Compliance Estimator

VSM variable stiffness mechanism

AFO ankle-foot orthosis

MR magnetorheological

ROM range of motion

PAM pneumatic artificial muscles

PPC push-pull cable

Abstract

The muscles around the ankle (calf and dorsal flexors) are essential for performing activities in daily life, like walking. Neurological and muscular pathologies, such as stroke, cerebral palsy, spinal cord injury, muscle atrophy and post-polio syndrome, affect the ability of voluntary muscle control and/or muscle strength of such muscles. This severely impairs the gait function of many people worldwide. An ankle-foot orthosis (AFO) or ankle brace, which is an assistive device that provides support to the ankle and foot, are in many cases a solution. Therefore, patients are fitted with an AFO to promote a functional gait pattern. To optimize the resulting gait pattern, the mechanical characteristics of the AFO should be matched to the specific malfunctioning muscles of a patient. This especially holds for the stiffness of the AFO. Generally, the AFO should be stiff enough to support the ankle's function, but also compliant enough to not restrict voluntary motion.

The optimal stiffness of an AFO for a patient can vary a lot, as the severity of the pathology differs and hence, the consequences, ranging from spastic to paralyzed muscles. It was found that issuing a sub-optimal AFO in the longer term may contribute to deterioration of physical function and gait. Thus, finding the optimal AFO joint stiffness for this group of patients and improving the speed of doing so, is an important clinical treatment goal.

Currently, this is achieved by a trial-and-error method consisting of fitting the patient with several orthoses. This method is time consuming and can possibly result in a sub-optimal AFO prescription. Ideally a human-in-the-loop setup is developed to find the AFO characteristics during tests using an AFO simulator. The corresponding AFO can then be fabricated and fitted to that specific patient. Hence, increasing the speed and quality of providing an AFO to a patient. However, current solutions are too expensive.

This assignment aims to create a proof of principle of a simplified, affordable, human-in-the-loop solution to vary the AFO stiffness, that enables clinicians to tune the AFO stiffness to a specific patient. This report describes the process of designing a lightweight AFO simulator with a continuously variable stiffness mechanism (VSM) and a predetermined torque-angle curve. The resulting design combines two key elements: A leaf spring of varying stiffness by changing the active length, and a cam part the serves as the transmission between the leaf spring and the AFO mockup. The design was fabricated and then validated with a dedicated AFO stiffness tester (BRUCE) based on manual deflection of the ankle-foot orthosis.

It was shown that the predicted plantarflexion stiffness range closely resembled the measured stiffness values. However, the measured dorsiflexion stiffness range was roughly two times smaller than predicted.

Concluding, the designed AFO simulator can change its stiffness, while being compact and lightweight. The potential of the design has been shown. Now it can be developed further into a fully functional AFO simulator system that can be worn by patients in a clinical gait laboratory setting.

Contents

1 Introduction

This section elaborates on the causes of disability, different categories of state-of-the-art AFOs, and on the study considerations. Finally, the proposed solution is presented.

1.1 Causes of disability

The human ankle plays an important role in performing activities in daily life. Neurological and muscular pathologies, such as stroke, cerebral palsy, spinal cord injury, muscle atrophy and post-polio syndrome, affect the ability of voluntary muscle control and muscle strength of muscles around the ankle joint. This severely impairs the gait function of many people worldwide [1]. The gait impairments are specifically caused by some form of spasticity and/or paralysis of the lower limb muscles. Of these pathologies, stroke is the number one cause of paralysis with 33.7% of all affected having to deal with some form of paralysis. Also, spinal cord injury (27.3%), multiple sclerosis (18.6%), and cerebral palsy (8.3%) have significant paralysis consequences [2], for an overview see Figure 1. Approximately 15 million people have a stroke each year worldwide, as stated in a report from the 'World Health Organization'. Furthermore, walking dysfunction occurs in more than 80% of stroke survivors [3]. Despite of rehabilitation efforts, approximately 25% of all stroke survivors have residual gait impairments that require full physical assistance before being discharged from the hospital [4]. Also, severe lower extremity injuries often lead to musculoskeletal weakness and pathological gait. As a result, the lower limbs ability to provide body support, forward propulsion, swing initiation, balance control, and foot clearance during swing is impaired [5], [6].

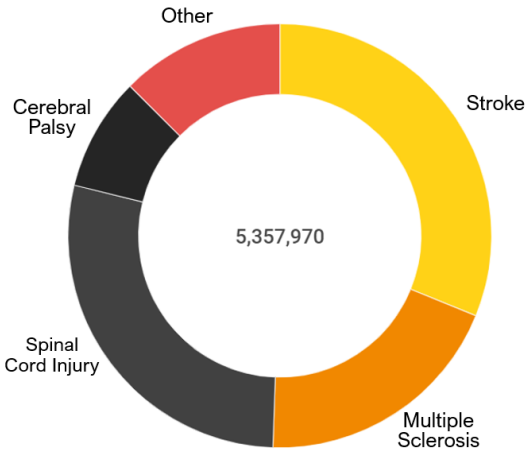

Figure 1: Prevalence of paralysis in the US (adapted from [7]).

1.1.1 Paresis and paralysis

Most neuromuscular disorders are characterized by paresis (weakness) or flaccid (complete) paralysis of the leg muscles. Paresis is a condition that causes a weakness of voluntary movement, or partial loss of voluntary movement. This is mostly due to neuromuscular recruitment patterns being disrupted, which consequently leads to certain muscles being relatively less active during a joint action. The paretic muscles are often lengthened, inhibited and weak. Flaccid paralysis means that no nerve supply occurs to the affected muscles. The paresis or paralysis of the plantar flexor muscles reduces the push-off power

that is essential to propel the body forward during the stance phase. Moreover, it results in a decreased walking speed and shorter stride length [8]. The paresis or paralysis of the dorsiflexor muscles results in inadequate lifting of the toes during the swing phase, which causes a drop-foot gait [9]. Foot-drop is one of the most common gait flaws. A person with a drop-foot suffers from toe-drag, foot slap, shorter step length, slower walking speed, higher metabolic cost, and a higher risk of tripping [10]. Therefore, patients with a paretic ankle usually have reduced walking capacity, resulting in a reduced participation in activities of daily living, which could affect the patient's quality of life [9].

1.1.2 Overactivity and spasticity

Another possible consequence of neuromuscular disorders is spasticity. Spasticity is characterized by certain muscles being continuously contracted. As a result, the muscles have an increased stiffness and tightness, and often inhibit normal movement, gait and speech [11]. Spastic paralysis is caused by the uncontrolled activities of the peripheral nervous system. Spasticity often comes with pain, soft tissue stiffness, joint contracture, may lead to abnormal limb posture, and increased caregiver burden [12]. If a muscle is only partly spastic, it can be called an overactive muscle. Which means a muscle can be more active during a joint action than it should be. Overactive muscles are characterized by being shortened, tight, and strong. A spastic condition is called problematic when the increased muscle tightness results in pain, positioning problems, impaired function, or increased care difficulties [13].

1.1.3 Summary

It is important to realize that the cause and the severity of gait impairment is different for each patient. Figure 2 shows this range muscle states. This means that there is not one optimal treatment that is most beneficial for everyone, resulting in challenges for clinicians helping these patients.

Figure 2: Muscle control can be in any state ranging from flaccid paralysis to spastic paralysis, with full muscle control in the middle.

To summarize the main possible consequences of neuromuscular disorders [14]:

1. Instability during standing and/or walking resulting in higher risk of falling.
2. Pain while standing and/or walking.
3. Decreased walking ability.
4. Reduced walking speed.
5. Reduced walking distance or walking time.
6. Increased energy consumption while walking.

1.2 State-of-the-art AFOs

To limit the aforementioned effects, AFOs are widely used, which is an assistive device that provides support to the ankle and foot. An AFO can increase the patient's ability to walk and improve their quality of life. Lower limb orthoses are the most commonly prescribed type of orthoses, with ankle–foot orthoses making up 26% of all orthoses provided in the United States [15]. The specific functions of AFOs can vary between assisting or resisting joint motion during the patient's gait, maintaining the correct alignment of a lower limb body segment, suppressing spastic and overpowered muscles and preventing or correcting deformities and protecting from external stimuli [16], [17]. Besides supporting unstable ankles and feet, some AFOs can also compensate for insufficient muscle function during key phases of the gait cycle. Several studies have shown that AFOs can provide assistance for patients with a paretic ankle for rehabilitation and help healthy people to reduce the metabolic cost of normal walking or loaded walking [9].

Most of the AFOs for rehabilitation purpose are designed to treat the drop-foot gait because the dorsiflexion muscles are more frequently affected as compared with the plantarflexion muscles [18]. Different kinds of AFOs have been developed such as the passive AFOs, semi-active AFOs, and active AFOs. These types will be discussed in the following subsections.

1.2.1 Passive AFO

Passive AFOs are normally made of a thermoplastic or composite in the form of a L-shaped brace. They can assist patients through inhibiting undesirable motions of the foot [9]. Common designs of passive AFOs include non-articulated thermoplastic types, such as a posterior plastic AFO, and articulate metal AFOs constructed from lateral metal uprights, hinges, foot holder, and straps [1]. These AFOs limit the foot posture and motion; thus, preventing undesirable conditions such as excessive foot rotation and toe drag. The material properties and geometry of the AFO influences its mechanical deformation properties and, thus, the amount of motion resistance (stiffness) it exerts on the ankle joint. However, because of the fixed construction of such AFOs, they also resist useful motions such as foot plantarflexion during the push-off phase. According to Ramstrand et al. [19], restricting the ankle joint motion might compromise important balance and postural control mechanisms during gait.

Compared to non-articulate AFOs, passive articulate AFOs can store energy during gait and provide assistance in dorsiflexion, adjust the initial angle of the ankle joint, and have better motion control using elements such as springs and oil dampers [20]. Passive articulate AFOs do not include any electrical elements or power sources [9].

1.2.2 Semi-active AFO

Due to the limitations of passive AFOs, semi-active AFOs are being developed by utilizing mechanisms like the magnetorheological (MR) brake or MR damper. The MR brake and MR damper use MR fluids. They can output a braking torque that can be controlled by controlling the current applied to them. With sensors, such as angle and force sensors, these AFOs can then modulate the compliance or damping of the AFOs based on the gait states and manage the motion of the paretic ankle, which can help solve some limitations of the passive AFOs. However, like passive AFOs, they also cannot provide active torque

to help the wearer to propel the body forward and reduce the metabolic cost of walking at the propulsive stage [9].

1.2.3 Active AFO

Quite different from the passive and semi-active AFOs, active AFOs can provide net power during gait. They make use of actuators and controllers and can generate controllable assistive torque for patients in both plantarflexion and dorsiflexion. Thus, active AFOs can help to propel the wearer's body forward during the propulsive stage of the stance phase. Enormous progress has been made in actuating, sensing, and performance of active AFOs in the past few years. However, there are no existing practical portable active AFOs for rehabilitation or metabolic cost reduction. Various technological challenges should be met to develop portable active AFOs. Some of the currently developed active AFOs are tethered with off-board components such as power supply and controllers [21], [22], [23], which make them not portable. Thus, they cannot be used for daily use. Furthermore, the untethered active AFOs [24], [25], [26], are often too heavy, even if the controllers and power supply are worn at the wearer's waist. To develop AFOs for future wide consumer adoption, they should improve in weight, actuator, and human-machine interface [9].

1.3 Study considerations

1.3.1 AFO focus area

Active and semi-active AFOs have received adequate attention but only a few solutions have made their way to practical implementation as daily support products. Thus, despite the disadvantages, passive AFOs are the ones that are being most widely used, as they are lightweight, reliable, durable, compact and economically viable [1], [27]. Therefore, the focus of this study will lie on doing research on passive AFOs. Specifically the focus will be on one of the most significant mechanical properties of passive AFOs: stiffness.

1.3.2 Stiffness' relevance

In order to know why stiffness in the ankle joint is an important characteristic of an AFO, one first has to understand what the plantar flexors and dorsiflexors do in a healthy person. Besides generating a plantarflexion moment around the person's ankle, the plantar flexors act eccentrically to control the rate and timing of the ankle's dorsiflexion. This function is important for controlling the rotation of the shank as well as influencing the energetics, kinetics, propulsion, support, and forward progression of gait [28], [29]. The dorsiflexors take care of toe clearance during the swing phase and prevent foot slap after heel strike. If for patients the plantar- and/or dorsiflexors are impeded, the right assistive stiffness at the ankle joint is key in normalizing their gait.

Excessively stiff dorsiflexion assist AFOs behave more like solid ankle AFOs. This subjects the user to an increased knee flexion moment that may threaten stance stability if the patient lacks knee or hip extensor strength. Furthermore, a study on non-pathological subjects demonstrated that a solid ankle AFO may requires 20% more activity of the quadriceps than an appropriate dorsiflexion assist AFO [30]. A study by Geboers et al. [31] concluded that people using an AFO after neurological damage risk further strength loss due to disuse. They found that issuing a sub-optimal AFO in the longer term may even contribute to deterioration of physical function and gait. Therefore, patients should be fitted with an AFO having the minimal ankle stiffness required to promote a functional

gait pattern, while being stiff enough for biomechanical control of ankle motion during gait.

1.3.3 AFO prescription process

So, how does the process currently look like of providing a patient with a customized AFO? The fitting procedure consists of three phases. In phase 1, the orthotist assesses the walking pattern of the patient and the neuromechanical characteristics of the ankle and calf. Phase 2 comprises of the design and fabrication of the AFO. If possible, in phase 3 the orthotist adapts and tunes one or more mechanical properties (e.g. stiffness, damping and alignment) of the AFO to fit a specific patient. The amount of stiffness of an AFO is typically estimated by the orthotist based on visual inspection of the patient's gait. There are no established methods for custom fabricating this type of AFO with predetermined ankle stiffness. An orthotic practitioner relies on trial and error due to an inability to anticipate the stress distribution in the orthosis. The exact stiffness is not known in advance of fabrication and is typically not measured afterwards. Because many orthoses are over- or under-engineered, they may not meet the biomechanical needs of the patient. So, finding the optimal AFO joint stiffness for this group of patients and improving the speed of doing so, are the main problems that should be solved.

1.4 Proposed solution

Upcoming techniques, like human-in-the-loop optimization, have proven to be able to tackle difficult, multi parameter optimization problems in exoskeletons for healthy humans. Furthermore, it could allow clinicians to deal with the AFO design and tuning problem in a closed loop configuration, which can continuously take the human-AFO interaction into account. For example, by changing the stiffness continuously during walking to find the optimum, resulting in correct stiffness for flexible rigid AFO design in a time efficient manner. For the US market such a human-in-the-loop system, the exoskeleton simulator (Caplex), is provided by Humotech, originally designed to mimic prosthetic feet. However, their orthotic functionality has some disadvantages like weight, undesired consequences of using Bowden cables and price. Therefore, this assignment will be the first step towards a human-in-the-loop setup that lets TU Delft researchers and its partners simulate the real-world physical characteristics of an AFO worn by a patient in a closed loop configuration.

The final goal is to enable clinicians to find the AFO characteristics that optimize the gait for a specific patient with impaired locomotion in a time-efficient manner. When these AFO characteristics are found during tests with the AFO simulator, the corresponding AFO can then be fabricated and fitted to that specific patient. This would highly increase the speed and quality of providing an AFO to a patient. This project from start to end falls outside the time range of one graduation project and is therefore cut into two. This project will focus on the first part, consisting of creating a proof of principle of a simplified, affordable, human-in-the-loop solution to vary the AFO stiffness.

2 Mechanical design

To design a system that effectively allows clinicians to find the optimal AFO stiffness for a specific patient before fabrication of their AFO, the system has to comply to certain criteria. First, these criteria are determined and listed. Second, the system specification section elaborates on the parts the system requires to meet these criteria in subsection 2.2. Then, in subsection 2.3 and subsection 2.4 the system is divided into subsystems and for each subsystem the possible design options are explained and compared. Third, the initial and final design combinations are put together and evaluated in subsection 2.5 and subsection 2.6 respectively. Fourth, the key elements of the final design are thoroughly explained in subsection 2.7. Finally, in subsection 2.8 the design and fabrication process of the proof-of-principle AFO simulator design are shown.

2.1 Criteria and metrics

First, the AFO simulator has to have a similar weight to that of actual AFOs. According to literature [32], [33], the weight of an AFO influences the patient's kinematics, kinetics, and metabolic cost. If the weight of the AFO simulator relatively differs too much from the commercially available AFOs, the stiffness value found through the AFO simulator will be different from a real AFO with a different weight. As described in section 1, many kinds of AFOs are available, ranging from passive AFOs to active AFOs. It has become clear that passive AFOs are the ones that are being prescribed most of the time. However, an important distinction must be made within the passive AFOs category: Namely, between articulate and non-articulate AFOs, also known as flexible rigid AFOs. Articulate AFOs have a freely rotating ankle hinge, in contrast to non-articulate AFOs. Non-articulate AFOs, which have a weight range of 140 grams to 600 grams [34], [35], [36], are prescribed more often than articulate AFOs. The articulate AFOs are often used for more complicated combinations of muscle states and have a weight range of about 800 grams to 1200 grams. These AFOs are mostly used for patients with calf muscle weakness and/or some form of lower limb spasticity. The stiffness of passive AFOs can range from 0.01 Nm/deg to about 25 Nm/deg (which is extremely rigid) [37]. However, the actual range of stiffness most of the time lies between 0.05 Nm/deg to 7.2 Nm/deg [38], [39].

To allow the clinician to find the optimal stiffness value for a specific patient, the stiffness must be able to be changed continuously. Also, the clinician should collect qualitative data to assess the consequences of each stiffness setting on the patient's gait. With this data the metabolic cost, kinematics and kinetics should be analyzed at each stiffness setting. However, to find the metabolic cost at a specific stiffness setting, patients would have to walk until the measured metabolic cost reaches a steady state. This can take multiple minutes due to a time delay between instantaneous energetic demand by the body and oxygen consumption measured at the mouth [40]. Therefore, as to minimize the time needed for the patient to walk on the treadmill, it is important that the stiffness can be changed while the patient is walking.

According to literature [41], [42] and as result from conversations with Yvette Kerkum and Peter de Groot of 'OIM Orthopedie' and with Niels Waterval of 'VUmc Amsterdam', the required ROM should be at least 40 degrees; 20 degrees dorsiflexion and 20 degrees plantarflexion. This ROM safely covers the ROM found in patients wearing passive AFOs. To summarize:

1. The AFO simulator stiffness must be continuously variable
2. The stiffness of the VSM must have the functionality to be changed during the patient's gait
3. The ROM must be at least 20 degrees dorsiflexion to 20 degrees plantarflexion
4. The weight of the AFO simulator should be lower than 1kg

Besides the criteria, the designed system will be judged on the difference between the measured and predicted stiffness range of the AFO simulator, hysteresis and backlash.

2.2 System specification

To control the stiffness of the AFO simulator, a variable stiffness mechanism (VSM) is required. This can potentially be integrated in the design or could be placed off-board to decrease the weight. In that case the forces have to be transmitted to the AFO simulator. To simplify the control of the physical characteristics of the AFO simulator the AFO simulator must be fixed in space. To realize real-time control, a computer is needed that can be operated by a person. Furthermore, the system needs to be able to collect data, so the operator knows how the physical characteristics are changing. To realize this, sensors need to be added to the test bench or to the AFO simulator. In Figure 3, a sketch is shown of how the setup of the AFO simulator system could look like.

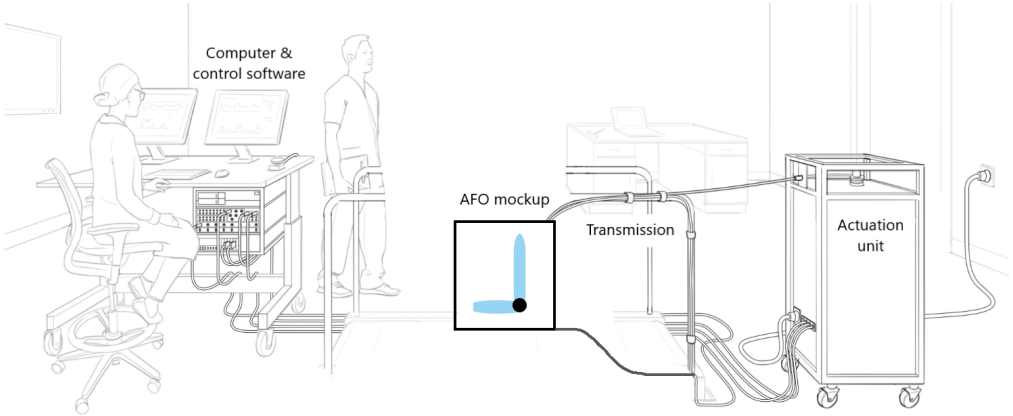

Figure 3: A sketch of the AFO simulator system setup (adapted from a figure made by Humotech).

Concluding, to meet the aforementioned requirements, the system should consist of the following parts:

1. A variable stiffness mechanism
2. A shank segment to which the VSM can be attached
3. A foot segment with a hinge connection to the shank segment
4. A test bench that is fixed in space and has sensors
5. A computer to process the measured data

In section 3, the chosen test bench and computer will be elaborated on. In the following chapter the design choices for the VSM, shank segment and foot segment will be discussed.

2.3 Morphological overview

First, to systematically choose the best design, a morphological overview is made. In a morphological overview the system is divided into subsystems each having a different function. The morphological overview can be found in Appendix B. Then, research is done to find possible options for each subsystem. To find these options regarding the VSM, the area of variable stiffness actuators was used. These systems closely resemble techniques that can be used to reach the goal of this project and are found in reviews in literature [43], [44], [45]. Second, each possible solution is reviewed and checked if it meets the criteria. Then, the options that are left are compared to each other, as to end up with the best solution. Finally, five feasible designs are put together and compared.

2.3.1 Variable stiffness mechanism

According to Ham et al. [43] to combine energy storage and adaptable compliance, an elastic element to store energy is needed. Many designs have been developed and can be divided into four categories.

Equilibrium controlled stiffness
Equilibrium controlled stiffness is used in certain compliant actuators. These actuators use a spring with a fixed stiffness in series with conventional actuation, like electric motors or hydraulic systems. For example, a series elastic actuator measures the displacement of the system and the force on the spring, and adjusts the torque supplied by the motor accordingly, which is also known as impedance control. To allow for variable stiffness, the virtual stiffness of the actuator is adjusted by dynamically adjusting the equilibrium position of the spring. A downside is that actuators that can exert enough force, are often too heavy.

Antagonistic controlled stiffness
A biologically inspired way to realize stiffness modulation is through the principle of antagonistic actuation [46]. An antagonistic actuator uses two motors to modulate the equilibrium position and the stiffness of a robot joint, like how the hamstrings and quadriceps muscles move the lower limb and modulate the stiffness of the knee joint, see Figure 4. For this kind of system to work, two actuators with compliance and nonlinear force-displacement characteristics need to be coupled antagonistically (working against each other). By controlling both actuators and using nonlinear springs, the compliance (and equilibrium position) of this antagonistic setup can be changed. Note that for the compliance to be varied in a controlled way, it is required that the spring characteristic of the two actuators is non-linear, so the resulting spring characteristic is linear [46].

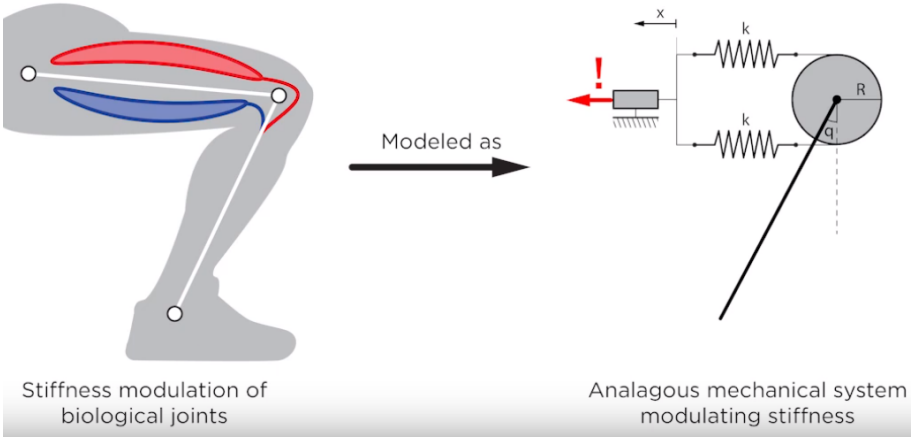

Figure 4: The antagonistic systems are inspired by the human musculoskeletal system [46].

An interesting example in the antagonistically controlled stiffness category, is the robotic joints that are actuated by McKibben muscles [47], also known as pneumatic artificial muscles (PAM), as they are relatively lightweight. Its overall shape looks like a thin cylinder which can contract by filling it with highly pressurized air. One of the drawbacks is the hysteresis resulting by friction, which makes it difficult to control. Moreover, it has a substantial threshold of pressure before any force is generated. The pleated PAM [48], reduces hysteresis and overcomes the threshold of pressure. Pneumatic muscles are actuators that are characterized by a high power-to-weight ratio and can be directly coupled to the joint without needing complex and heavy gearing mechanisms. The drawbacks of a joint actuated by two pneumatic muscles are the nonlinear characteristic of the joint, slow dynamics (especially depressurizing the muscle is slow), presence of hysteresis, and need for pressurized air [45].

Structure controlled stiffness
In contrast to the previous two categories, structure controlled stiffness systems modulate the effective physical structure of a spring to change the stiffness. When using a beam as elastic element, the stiffness depends on the material modulus, the moment of inertia, and the effective beam length. The stiffness can be controlled by adjusting one of these characteristics [43]. For example, the Jack Spring Actuator [49], of which the compliance adjustment is achieved by adding or subtracting the number of available coils used in a spring. A lever mechanism of which the effective length can be changed is also possible. A lever has three principal points: the pivot, the spring attachment point, and point to where the force is applied. By changing the position of one of these parameters a variable stiffness mechanism independent from the equilibrium position is created. The lever method produces energetically efficient stiffness adjustment since the displacement needed to change the stiffness is perpendicular to the force generated by the springs. A disadvantage is that most of the time the passive joint range is limited compared to other designs [45].

Mechanically controlled stiffness
Comparable to structure controlled stiffness, mechanically controlled stiffness systemss also alters the effective physical stiffness of the system. However, the full length of the spring is always in use. In this category the variation is done by changing the pretension

of the spring. Examples of actuators which use this technique are the 'mechanically adjustable compliance and controllable equilibrium position actuator' (MACCEPA) [50] and the variable stiffness joint [51]. These actuators only need one compliant element. The complete actuator behaves as a torsion spring where the spring characteristics and equilibrium position can be controlled independently during operation.

2.3.2 Other subsystems

Location VSM
For this project it is important that the weight of the AFO simulator is as small as possible so the AFO simulator affects the gait of the patient minimally, while providing the desired joint stiffness. Therefore, to avoid unnecessary loads on the transtibial lower limb and the foot, actuators could be placed off-board, around the waist or in a backpack [52]. Only some systems qualify for being partly on the lower limb due to their low weight, like PAM, hydro muscles, or a leaf spring.

Transmission
The transmission subsystem describes the possibilities on how to transfer energy to the AFO simulator in order to simulate stiffness. As the goal is to be able to modulate the stiffness while the patient is walking on a treadmill, the transmission needs to move along with the lower limb of the patient. A way to do this is by using a flexible transmission. One of the most used flexible transmissions are Bowden cables. Other types of transmission have been proposed, like in-extensible cords, open-ended cables, endless cables, and push-pull cables (PPC) [52]. In contrast to Bowden cables, that are only able to transfer pulling forces, PPCs are bi-directional, meaning they can transfer force in both pulling and pushing directions. However, consequently PPC cables are larger in diameter, stiffer and heavier. Moreover, according to a study performed by Grosu et al. [53], the typical disadvantages for cable-based transmissions are also characteristic to PPC actuation. Still, PPC actuation could be preferred due to the number of individual advantages in certain applications. For example, the capability to transfer larger forces in two directions and less complex mechanical construction of the actuation system.

In previous years, cable-based actuation got increased attention in rehabilitation robotics [54], [55], [56], which is mainly due to advancements in the strength of cable materials. The cable materials support the transmission of high forces and offer the possibility of locating actuators away from the patient. However, these advantages could be overshadowed by the nonlinear dynamic behavior caused by friction between the cable and the cable housing. Also, backlash can occur due to compliance and friction in the cable housing when the direction of the actuation changed. This issue can result in a decrease in control precision and has to be compensated for with control algorithms [53].

Stiffness adjustment
For this project, the stiffness was planned to be adjusted manually. Several options were evaluated: pulling a lever, turning a winch, rotating a screw mechanism or any other manual way that would let the researcher change the stiffness of the AFO simulator. These mechanisms are compared in subsubsection 2.4.3 and sketches of these mechanisms can be found in Appendix B.

Foot and shank segment
For the foot and shank segment a stiff and simple design should be chosen, as the focus

should lie on the VSM. The stiffer and lighter the AFO simulator is, the less it influences the behavior of the VSM. During a certain stage of the design process, it seemed more realistic to manufacture an actual AFO in time instead of making a proof-of-principle design of the system. Therefore, the option to choose between a real AFO or a proof-of-principle design was added to the morphological overview.

Conclusion
In Appendix A the pros and cons of each subsystem can be found. Whenever a con is colored red, it means that that specific con either causes that subsystem to not meet the set criteria or that it has a disadvantage that is too significant. In the following chapter the possibilities that are left, are compared.

2.4 Comparison of most promising options for subsystems

Following from the previous pros and cons of each subsystem, some are not suitable for reaching our objective. The ones that are, will be compared in this chapter.

2.4.1 Antagonistic mechanism vs changing the active leaf spring length

The most promising ways to vary the stiffness of the AFO are the antagonistic mechanisms and the structure-controlled stiffness mechanisms, with changing the active length of a leaf spring in specific. The antagonistic mechanisms often need to be placed offboard, to meet the weight criteria. The leaf spring mechanism compared to the antagonistic mechanism has a larger stiffness range and requires a smaller force to change the stiffness, as can be seen in Figure 5.

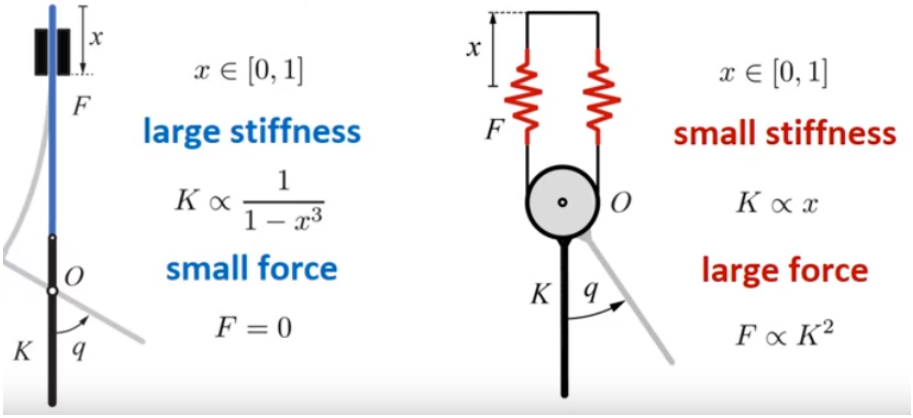

Figure 5: The properties of a) a variable lever length mechanism and b) an antagonistic mechanism.

Moreover, the leaf spring mechanism has less parts and does not have to deal with asymmetry. On top of that, the antagonistic subclass uses nonlinear springs, which is often a drawback and the antagonistic springs also reduce energy efficiency and energy storage capacity [57]. Researchers, like Hurst et al., abandoned the antagonistic setup as it significantly reduced energy storage capacity. This is due to energy having to be transferred from one spring to another instead of directly to the joint [45]. A disadvantage of the leaf spring mechanism is that it has a smaller range of motion than the antagonistic setup. However, in our case the required range of motion is relatively small. Concluding, for this project the leaf spring mechanism is most suitable.

2.4.2 Cable-based vs hydraulic based transmission

If a transmission is chosen in one of the design combinations, a comparison has to be made between transmission through cables and hydraulic transmission. In 1985, Leblanc [58] did research on flexible force transmission in body-powered upper-limb prostheses. He tested steel and plastic cables with either a steel, steel with Teflon liner, or a plastic housing and a hydraulic master slave transmission using cylinders. The plastic cable riding in the Teflon-lined steel housing offered the highest efficiency of cable systems tested, being 90% at 180 degrees and 81% at 360 degrees of cable routing. On the other hand, the hydraulic system offers a constant 90% efficiency over any routing of the hydraulic line. Therefore, for situations where a cable must be routed through greater than 180 deg, the hydraulic system is superior in efficiency. However, for this project, the angle of routing should never be greater than 90 degrees. The figure shows that a plastic and steel cable in a Teflon liner offer the highest efficiency ranging from 99% at 0 degrees, to 95% at 90 degrees, which is better than the hydraulic system. Finally, other disadvantages are the need for precisely custom manufactured pistons, leaks, and the weight of the pistons. Concluding, the cable-based transmissions are best fit for this project.

2.4.3 Stiffness adjustment comparison

For this project the stiffness will be adjusted manually. First, a screw mechanism could be used, which has the advantages of being self-locking, cheap, and able to continuously vary the stiffness. Second, a lever mechanism is possible. It can be bought off-the-shelf, is self-locking and on top of that, can also change the stiffness continuously. However, it may be hard to change the stiffness with precise amount and the maximum cable displacement is limited. The third option, a wheel, has a problem of not being self-locking by default. An extra mechanism would be needed to lock the wheel. A possible solution could be to use a hand winch. The hand winch is compact, can be bought off-the-shelf, can change the stiffness in small discrete steps and is cheap. However, it is only self-locking in one way. Concluding, the self-locking capability in both ways of the screw mechanism is most suitable for changing the stiffness of the AFO simulator.

2.5 Initial design combinations

As a result of the comparisons made between all options for all subsystems, five initial designs have been put together, see Figure 6. In this chapter, the weight and other characteristics of these five designs are compared.

Subsystem	Design options				
	1a	1b	2a	2b	2c
VSM	Vary active length leaf spring	Vary active length leaf spring	Vary active length leaf spring	Vary active length leaf spring	Vary active length leaf spring
Location VSM	Offboard	Offboard	Onboard	Onboard	Onboard
Transmission	Push-pull cable	Push-pull cable	Wireless	Push-pull cable	Bowden cable
Stiffness adjustment	By hand	By hand	Actuator	Rotate screw	Rotate screw
Cable attachment point	Anterior	Posterior	-	Posterior	Posterior

Figure 6: The five initial designs consisting of the most promising options for each subsystem.

2.5.1 Weight comparison

First, the weight of each design, which is one of the most important characteristics, is compared. The buildup of the total weight of each design can be seen in the Table 1.

Parts	Design options				
	1a	1b	2a	2b	2c
	(in g)	(in g)	(in g)	(in g)	(in g)
Transmission cable	330	400		250	50
Structure	400	400	400	400	400
Leaf spring			70	70	70
Motor + gearhead + encoder			67		
Lead screw + spring support + bearing			50		
Electronics + box			86		
Battery + SOC			78		
Slider			38	38	38
Slider spring					20
Other hardware	30	30	30	30	30
Total weight	**760**	**830**	**819**	**788**	**608**

Table 1: Weight estimate of the five initial design options.

One of the most surprising findings was the weight of the PPCs. Depending on the force the PPC needs to transfer, the PPC differs in size and weight, ranging from 200 to 400 grams. These weights are caused by the PPCs having rigid tubes on both sides to facilitate the push function of the cables. Therefore, their weight almost nullifies the advantage of the VSM being located offboard. The exact values for the weight of the components of design 2a, are based on the weight of these components in the variable stiffness prosthesis of Shepherd et al. [59] and function as an estimation of the weight of those parts of the design. The actuator that is required to move the slider in design 2a is lightweight, as the

torque requirements are low due to the leaf spring almost being fully unloaded during the patient's swing phase. As in design 2c a Bowden cable is used instead of a PPC, a spring is added to the design, so the slider is able to return to the stiffest position at the bottom of the VSM. The winner in the weight comparison is design 2c, with an estimated total weight of 608 grams.

2.5.2 Characteristics of each design

In this chapter the characteristics of each design are compared, see Table 2.

Characteristics	Design options				
	1a	1b	2a	2b	2c
Hysteresis	Yes	Yes	No	No	No
Stick-slip effect	Yes	Yes	No	No	No
VSM on rails	Yes	Yes	No	No	No
Needs a test shoe	Yes	No	No	No	No

Table 2: Characteristics of the five initial design combinations.

First, it is shown that the VSM can be mounted to the AFO simulator without adding too much weight. In that way the disadvantages of a flexible force transmission can be avoided. This would simplify and increase the performance of the system. In that case, the leaf spring would be directly connected to the AFO simulator, so that the stiffness of the leaf spring is directly transmitted to the patient's foot. Moreover, in the case of the VSM being located offboard, it has to be able to slightly move with the patient, as not every patient will walk on the same position on the treadmill. This is needed as a PPC cable only properly works when the cable routing is constant throughout the tests. A solution for this would be to put the VSM on a rail. However, if the VSM is attached to the AFO simulator, the flexible transmission cable can be a bit longer, avoiding the need for the VSM being attached to a rail. Therefore, option 1a and 1b, can't stand up to the variations of option 2. Then, looking at the variations of option 2, design 2b and 2c have a major problem. Their way of adjusting the slider position is unable to lock the slider firmly into place. The slider needs to be able to be locked at each stiffness setting, as the leaf spring will exert a force in the y-direction, pushing the slider up. Design 2a does have this self-locking property, as the slider is connected to lead screw which is non-backdrivable (if the pitch is sufficiently small). Concluding, design 2a has a sufficiently low weight, avoids the disadvantages of a flexible force transmission (hysteresis and stick-slip effect) and allows the position of the slider to be self-locking. In the following chapter, design alterations of design 2a are presented and compared.

2.6 Final design combinations

In this chapter the weight and other characteristics of design 2a and its design iterations are presented and compared, see Table 3.

Subsystem	Design options			
	2a1	2a2	2a3	2a4
VSM	Vary active length leaf spring	Vary active length leaf spring	Vary active length leaf spring	Vary active length leaf spring
Location VSM	Onboard	Onboard	Onboard	Onboard
Stiffness adjustment	Actuator	Actuator	Actuator	Actuator
Location stiffness adjustment	Onboard	Onboard	Waist	Offboard
Transmission	Wireless	Wireless	Flexible rotary shaft	Flexible rotary shaft
Location electronics	Onboard	Waist	Waist	Offboard

Table 3: The four final design iterations.

2.6.1 Weight and characteristics

The buildup of the total weight around the ankle of each design can be seen in Table 4.

Parts	Design options			
	2a1	2a2	2a3	2a4
	(in g)	(in g)	(in g)	(in g)
(bowden/PPC/rotatry)			20	20
Structure	400	400	400	400
Leaf spring	70	70	70	70
Motor + gearhead + encoder	67	67		
Lead screw + spring support + bearing	50	50	50	50
Electronics + box	86			
Battery + SOC	78			
Slider	38	38	38	38
Slider spring				
Other hardware	30	30	30	30
Total weight	**819**	**655**	**608**	**608**

Table 4: Weight of design options. Note: Weight of structure is a rough estimate.

The design iterations of design 2a have a lower weight. Components that were on the AFO simulator before, are now attached around the waist or placed offboard. Design 2a2 has 164 grams around the waist, design 2a3 394 grams and design 2a4 about 80 grams. The advantages of a flexible transmission and the self-locking characteristic of the slider on a lead screw are combined to form a solution that is best of both worlds: a flexible shaft. A flexible shaft is made to transfer torque over a distance in both directions. This results

in the actuator being able to be placed at the waist or offboard while still being able to change the position of the slider by turning the lead screw. Flexible shafts in general are 85 to 95% efficient, which is typically better than gears, universal joints, and belts and pulleys, which lose efficiency because of higher frictional losses. Moreover, they have a 3 to 1 weight advantage over these other design options. They are used extensively in the aerospace, medical, automotive, and other industrial markets [60]. A flexible shaft of 90 cm has a weight of approximately 160g, but can be almost nullified by letting the cable go through a belt loop of the patient. Then, when comparing design 2a3 and 2a4, design 2a3 could also be used outside the lab, while still having the same weight around the ankle of the patient as design 2a4. Concluding, design 2a3 is the best performing design, as it has the lowest weight and most advantages.

2.7 Final design

In this chapter the final design, that is inspired by a variable stiffness prosthetic ankle [59], will be described in detail and each key element will be thoroughly explained.

The design combines two key elements: A leaf spring of which the stiffness can be varied by changing the active length, and a cam part the serves as the transmission between the leaf spring (which is part of the VSM) and the AFO simulator. The cam part can be designed in such a way, that the resulting torque-angle curve of AFO can be customized to any shape. When the ankle of the AFO simulator rotates, the cam follower rolls along the cam profile, which causes a deflection of the leaf spring. The active length of the leaf spring can be varied, by changing the position of a slider by using an actuator and a flexible shaft. However, for this project the focus will lie on testing the VSM by creating a proof-of-principle of the AFO simulator, therefore the lead screw will be manually turned by using a winged nut. The slider serves as the pivot point of the leaf spring. Altering the stiffness of the leaf spring changes the torque-angle curve at the ankle, decreasing or increasing the stiffness. Even though, the torque-angle curve will become stiffer or less stiff, the shape of the curve stays the same. A figure made by Shepherd et al. [59], Figure 7, shows clearly what steps must be taken to predict the AFO stiffness range and what shape the torque-angle curve is going to have.

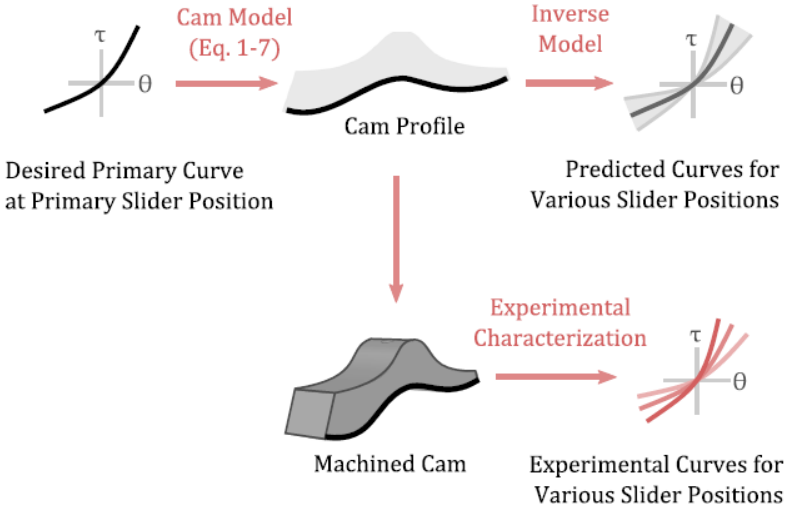

Figure 7: First, a cam shape is mathematically derived. Second, an inverse model is created to predict the range of torque-angle curves that would be available. These curves are then compared to experimental data.

2.7.1 Desired primary torque-angle curve

First, a desired primary torque-angle curve has to be chosen. Our goal for the AFO simulator is to have a behavior that is as similar as possible real AFOs. Most passive AFOs have a linear torque-angle curve, hence the desired primary torque-angle curve will be linear. The primary slider position was chosen to be at 50% of its range of motion, to allow an appropriate range of stiffer and less stiff torque-angle curves.

2.7.2 Cam transmission

Rotation of the ankle joint creates a sideways deflection of the free end of the leaf spring, through a rolling cam transmission. The deflected leaf spring in turn creates a restoring torque at the ankle joint. The cam profile determines the torque-angle curve at the ankle. A cam profile can be created for virtually any arbitrary desired torque-angle curve. The purpose of this section is to provide the mathematical equations to convert a desired primary torque-angle curve at a desired slider position to the corresponding cam profile. These mathematical steps can also be found in the paper by Shepherd [59].

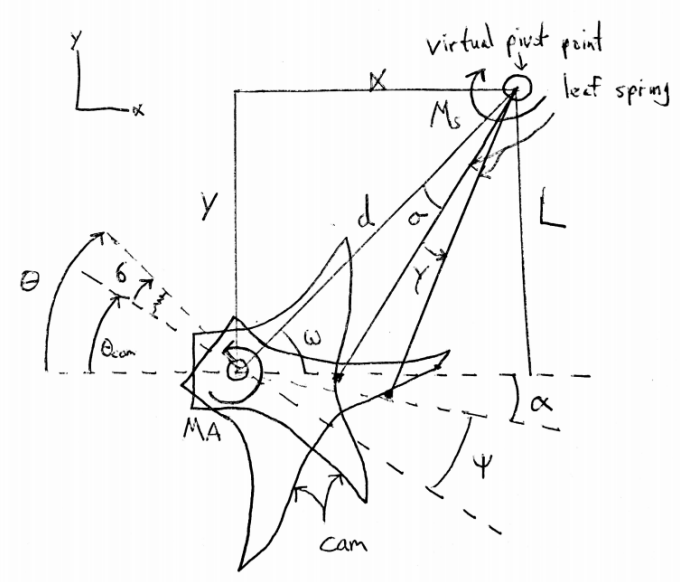

Figure 8: A sketch that shows the geometrical variables of the key elements of the system (adapted from a figure by Shepherd [59]).

Where γ is the angular deflection of the leaf spring, M_S is the moment caused by the spring, θ is the ankle angle, M_A is the ankle torque and δ is the series compliance of the frame.

The problem is solved using the principle of virtual work. That is, assuming no energy loss in the transmission or spring. In that case the energy stored in the ankle minus the energy stored in the series compliance is equal to the energy stored in the leaf spring:

$$\int_0^{\gamma} M_S d\gamma = \int_0^{\theta} M_A d\theta - \int_0^{\delta} M_A d\delta \tag{1}$$

The right side of Equation 1 is partly known as a function of θ. The desired torque-angle curve is specified at the ankle and can thus simply numerically integrate the desired torque-angle curve as the series compliance can be estimated. For simplicity, dorsiflexion and plantarflexion are solved individually, so the lower limit of integration is 0. At the equilibrium position $\theta = 0°$, the spring has a pretension that is denoted with γ_0. Equation 1 can be rewritten to:

$$\int_0^{\gamma} k\left(\gamma + \gamma_0\right) d\gamma = \int_0^{\theta} M_A d\theta - \int_0^{\delta} M_A d\delta \tag{2}$$

Here k is the rotational stiffness of the leaf spring. The left side of this equation can be integrated to:

$$\frac{1}{2}k\gamma^2 + k\gamma_0\gamma + c = \int_0^\theta M_A d\theta - \int_0^\delta M_A d\delta \tag{3}$$

where the constant of integration, C, is found to be zero from the initial conditions: $\theta = 0$, $\gamma = 0$. The quadratic formula is then used to solve for γ as a function of θ

$$\gamma(\theta) = -\gamma_0 + \sqrt{\gamma_0^2 + \frac{2}{k}\left(\int_0^\theta M_A d\theta - \int_0^\delta M_A d\delta\right)} \tag{4}$$

Where γ, the leaf spring angle, is denoted as a function of the ankle angle θ of which both integrals can be evaluated numerically. The radius of the cam profile can be derived as a function of θ, from γ and the defined geometry using the law of cosines:

$$r(\theta) = \sqrt{L^2 + d^2 - 2Ld\cos(\gamma + \sigma)} \tag{5}$$

Finally, to have a polar representation (r,ψ) of the cam profile in the cam reference frame, ψ is needed as a function of θ:

$$\psi(\theta) = \theta_{cam} - \alpha = \theta - \delta - \alpha \tag{6}$$

α, the small deviation from horizontal, can be found by using the law of sines:

$$\alpha(\theta) = \sin^{-1}\left(\frac{L}{r(\theta)} \cdot \sin(\sigma + \gamma(\theta))\right) + \omega \tag{7}$$

The numerical results are now in polar coordinates as (r,ψ). This curve is converted to Cartesian coordinates, and a parallel curve corresponding to the final cam profile is created with a perpendicular offset equal to the cam follower radius. The calculations are slightly different for creating the torque-angle curve in plantarflexion direction as Equation 6 changes to:

$$\psi(\theta) = \theta_{cam} = \theta - \delta \tag{8}$$

And an extra variable ϕ is added to describe the new angle:

$$\phi(\theta) = \psi + \alpha \tag{9}$$

The resulting cam shapes for both dorsiflexion and plantarflexion are shown in Figure 9a and Figure 9b respectively.

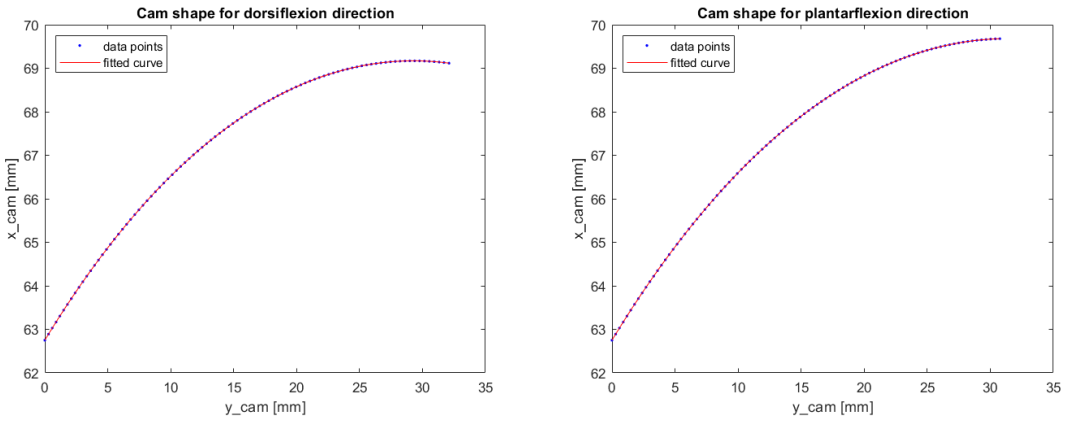

(a) (b)

Figure 9: (a) The cam shape for dorsiflexion direction and (b) cam shape for plantarflexion direction.

Then, the following steps have to be taken to create the cam in SolidWorks:

1. Create dorsiflexion cam shape in MATLAB and note the end points.
2. Create plantarflexion cam shape in MATLAB and note the end points.
3. Copy dorsiflexion cam shape formula in SolidWorks and mirror it.
4. Copy plantarflexion cam shape formula in SolidWorks.
5. Create a linking line with radius of the cam follower.
6. Connect the dorsiflexion and the plantarflexion cam shape to the linking line and make them tangent.

The resulting SolidWorks model of the cam is shown in Figure 10.

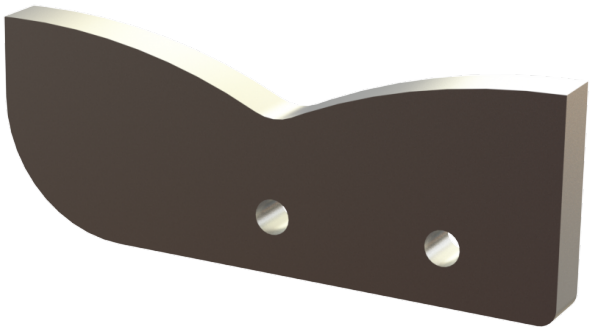

Figure 10: SolidWorks model of the cam part.

An inverse model was also created, which returns the torque-angle curve at the ankle for a given cam profile and slider position.

2.7.3 Leaf spring

A VSM based on a leaf spring realizes a variable transmission by changing the lever arm ratio between the two parts of the leaf spring, which is done by moving the pivot point along the leaf spring. The equations presented in this section use approximations for small output deflections, but still offer a good representation of the leaf spring with pivot mechanism and are a useful tool for analysis. This section also looks at how leaf springs can be designed in such a way that their energy storage capacity is maximized while minimizing their mass. The steps taken in a paper by Barret et al. [61], who did research on the elastic energy storage in leaf springs, are followed.

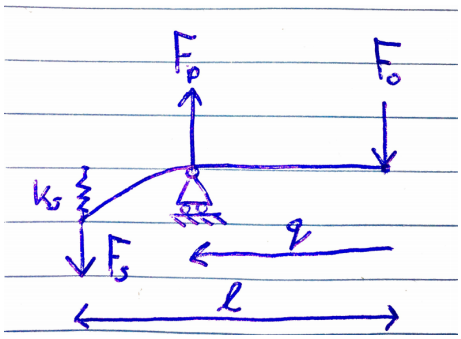

Figure 11: A free body diagram of the leaf spring.

The equations that follow, are derived for straight beams, where l is the total length of the leaf spring, and q the distance from the slider to the end of the leaf spring. Following from Figure 11, the internal forces on the leaf spring at the base, end and pivot are:

$$F_s = k_s \cdot s, \quad F_o = \frac{l-q}{q} \cdot F_s, \quad F_p = F_s + F_o = \frac{l}{q} \cdot F_s \tag{10}$$

Where k_s is the linear stiffness of the leaf spring, F_s is the force at the end of the leaf spring, F_p the force at the pivot point and F_o the force at the base of the leaf spring. In the proof-of-principle design section, the maximum values of these forces will be used to design parts that are strong enough.

Then, leaf springs can be modeled as an Euler-Bernoulli beam, assuming that the beam is slender and has small deflections $w(x)$, where x is the distance from the spring's end along its neutral fiber. For the simple case of a beam with constant, rectangular cross section with width b and thickness h, area moment of inertia $I = \frac{bh^3}{12}$, and the constant flexural modulus E, that has one fixed end, and that is loaded with the force F at its free end; the maximal deflection at the end of the leaf spring is:

$$w(0) := s = \frac{F \cdot l^3}{3 \cdot E \cdot I} = \frac{4 \cdot F \cdot l^3}{E \cdot b \cdot h^3} \tag{11}$$

The stiffness of the spring can be described by rewriting Equation 11 and taking the derivative of F with respect to s:

$$k = \frac{dF}{ds} = \frac{3EI}{l^3} = \frac{Ebh^3}{4l^3} \tag{12}$$

The maximum energy that can be stored in the spring now depends on the maximum spring deflection, achieved when the stress in the spring reaches its permissible limit. The

maximum bending stress occurs at the surface of the fixed end of the beam, where the moment $M_b(l)$ is largest.

$$\sigma_{\max} = \frac{M_b(l)}{I}\frac{h}{2} = \frac{6Fl}{bh^2} \tag{13}$$

Which can be rewritten to:

$$F = \frac{\sigma_{\max} bh^2}{6l} \tag{14}$$

Then, substituting this in Equation 11, gives the maximum deflection:

$$s_{\max} = \frac{2}{3}\frac{l^2}{h}\frac{\sigma_{\max}}{E} \tag{15}$$

Finally, the maximum energy that can be stored in the spring is

$$\begin{aligned} W_{b\,\max} &= \tfrac{1}{2} F s_{\max} = \tfrac{1}{2} k s_{\max}^2 \\ &= \tfrac{1}{2}\frac{Ebh^3}{4l^3}\left(\tfrac{2}{3}\frac{l^2}{h}\frac{\sigma_{\max}}{E}\right)^2 \\ &= \tfrac{1}{9}\frac{\sigma_b^2}{2E_b} bhl = \eta_A \frac{\sigma_b^2}{2E_b} V \end{aligned} \tag{16}$$

With the degree of volume utilization $\eta_A = 1/9$,, specific energy absorption capacity $\frac{\sigma_b^2}{2E_b}$ and volume $V = bhl$. The degree of volume utilization η_A, or form coefficient C_F, accounts for a non-uniform stress distribution, comparing the actual energy stored in the material with the highest possible energy stored in the same volume. Higher values of energy absorption capacity indicate that materials can store higher levels of elastic energy without yielding and are therefore better candidates for springs. The specific energy capacity $\frac{W}{V} = \frac{\sigma^2}{2E}$ is quadratic to the elastic limit of the material, and inversely proportional to its elastic modulus, meaning that though, i.e. strong and elastic, materials are required. The length of the leaf spring is chosen to allow for a sufficient stiffness range, which in this case is about 180mm. The width of the leaf spring is chosen to ensure the leaf spring to be wide enough for the cam transmission to be passing through, which is 20mm.

For the final system the shape should be chosen in such way that the form utilization is maximized, for example by giving the leaf spring a parabolic height. However, in this project the leaf spring will not be loaded to its limits, as the stiffness range is lower than it will be in the final system. Therefore, a standard rectangular cross section is chosen. Using CES Edupack the materials are found with the highest elastic potential energy and the lowest weight and are shown in Table 5.

Material	Elastic stored energy (J/m^3)	Average elastic stored energy (J/m^3)	Density (kg/m^3)	Weight factor	Ranking
Aluminium, 7075, T6	9.2e5 - 1.88e6	1.78E+06	2800	3.29	3
Epoxy/HS carbon fiber (woven prepreg)	2.3e6 - 4.4e6	3.35E+06	1600	1.00	1
Titanium alloy (e.g. Ti-6Al-4V)	4.49e6 - 5.12e6	4.80E+06	4400	1.92	2
Spring steel C75 (1.1274)	1.88e6 - 2.79e6	2.35E+06	7900	7.04	4
Stainless steel spring steel (AISI 301, annealed)	9.81e4 - 1.4e5	1.19E+05	7900	139.00	5

Table 5: Leaf spring material candidates found in CES Edupack.

The combination of the energy capacity, density and weight of carbon fiber is most favorable to serve as leaf spring material. The weight factors show how much heavier the leaf spring made from another material needs to be to achieve the same elastic potential energy. Surprisingly, 7075 aluminum is better suited to be used as leaf spring material than spring steel, as it is lightweight and still has a decent energy-storage capacity. Moreover, 7075 aluminum is readily available in the workshop of the TU Delft and was therefore chosen as the leaf spring material for the AFO simulator.

Finally, the height was iteratively found using a MATLAB script so that the leaf spring would be strong enough, for when the slider is put in the stiffest position, and to still allow AFO simulator to reach its maximum ROM. The resulting spring design can be seen in Figure 12.

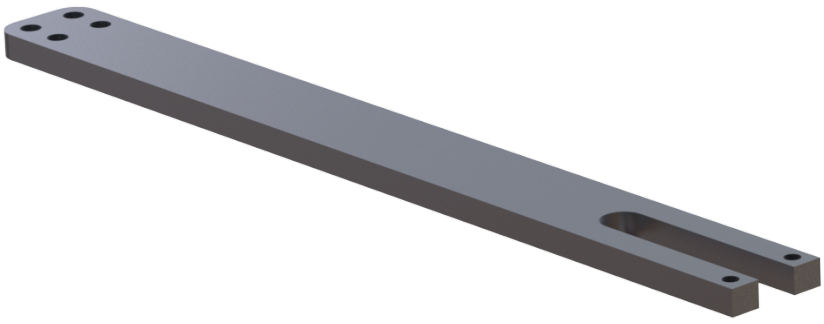

Figure 12: SolidWorks model of designed leaf spring.

2.8 Design of a proof-of-principle version of the AFO simulator

Now that the key components are designed, the design for the AFO body and parts of the VSM will be elaborated on in this chapter. It was decided to lower the desired stiffness range, so most parts could be 3D printed using PLA. This allowed me to construct a prototype in a time-efficient manner during Covid-19, which could be made from off-the-shelf parts, 3D printed parts and some CNC'd parts.

2.8.1 Variable stiffness mechanism

The VSM consists of the following parts:

- Slider
- Lead screw
- Two angular contact ball bearings
- VSM base
- Cam follower
- Cam follower to leaf spring connector

First, according to research conducted by Letcher [62], 3D printed parts made from PLA with a 100% infill have an average ultimate stress of 58.45 MPa and an average modulus of elasticity of 3.33 GPa. Using these estimations of the material properties the dimensions of the 3D printed parts were chosen accordingly. The VSM base consists of three 3D printed parts. To the top part the leaf spring has to be attached, the ball bearing has to be secured and the top clamp has to be attached. The bottom part of the VSM base only needs to have a ball bearing and be able to be secured to the bottom clamp. A design was made that is suitable to be 3D printed, by taking the printing orientation into account, cutting sharp corners and by choosing correct 3D print tolerances. The top and bottom part of the VSM base were connected with a rectangular part, that minimizes the bending moment on the ball bearings which is caused by the weight of the surrounding parts. The lead screw is 180mm long, has a diameter of 10mm made and is made from C45 steel. The lead screw dimensions are chosen in such a way, that the middle of the lead screw will never deflect more than one tenth of a millimeter. Resulting from the calculations done on the lead screw, the ball bearings need to have a static load rating of at least 1100N. To be on the safe side, angular contact ball bearings with a static load rating of 2440N were chosen. Their outer diameter is 22mm and inner diameter is 8mm. The lead screw is glued to the ball bearing with Loctite. The slider casing was also 3D printed and made so a machined steel nut could be sunk into it. Also, a 5mm silver steel shaft could be press fitted in the slider casing. The slider is re-positioned by turning a winged nut at the top of the lead screw. The silver shaft can then slide over the surface of the lead spring whenever the position of the slider needs to be changed. The cam follower consists of a needle bearing with an outer diameter of 9mm and an inner diameter of 5mm. The needle bearing was slid on a 5mm diameter silver steel shaft. This shaft was pressed into a 3D printed part that was screwed to the end of the leaf spring. Calculations were done to choose appropriate dimensions for each of these parts. In Figure 13 the resulting assembly of the VSM can be seen.

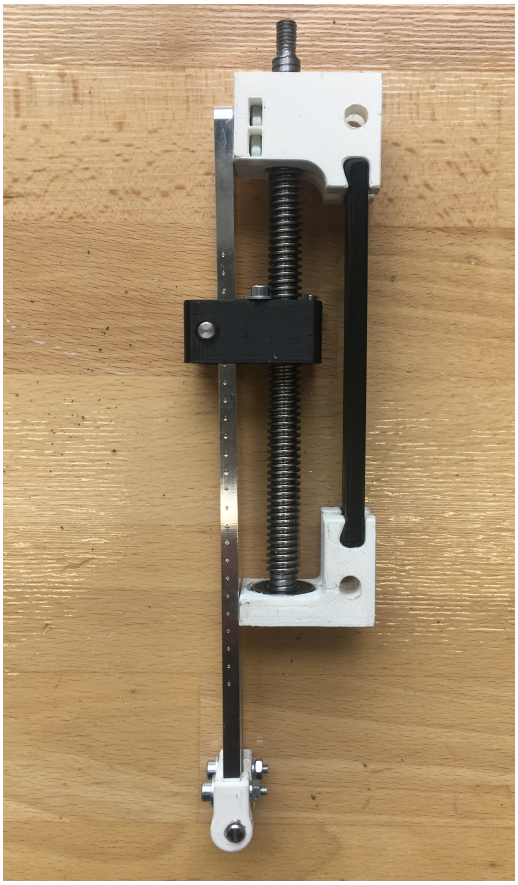

Figure 13: VSM of the proof-of-principle design.

2.8.2 AFO simulator body

The body of the AFO simulator consists of the following parts:

- Foot segment
- Top clamp
- Bottom clamp

The function of the top clamp is to attach the top part of the VSM to the shank segment of the testing device, BRUCE. Similarly, the bottom clamp attaches the bottom part of the VSM to the shank segment of the BRUCE and forms the bridge between the VSM and the foot plate. The foot plate is clamped between the base plate and the dummy foot of the BRUCE. The cam transmission is mounted on the back of the foot plate and secured using two M4 nuts and bolts.

2.8.3 Assembly

Two orientations of the resulting design are shown in Figure 14a and Figure 14b.

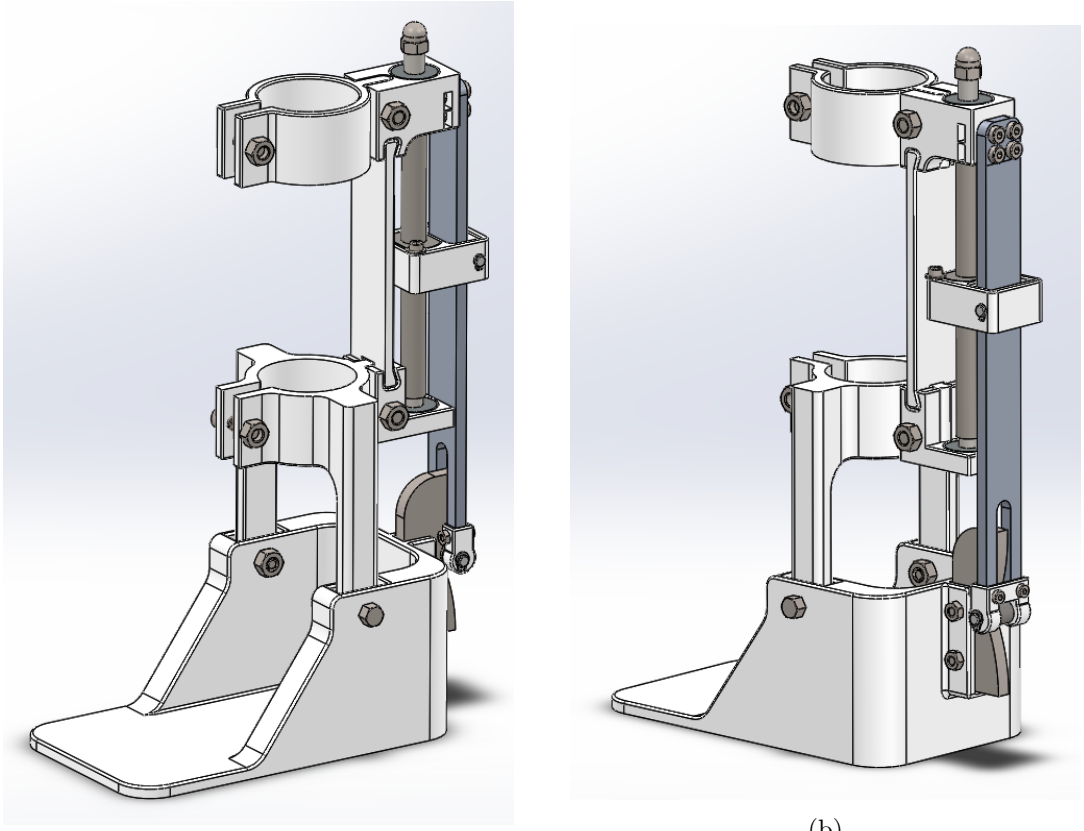

(a) (b)

Figure 14: (a) A front trimetric view of the final AFO simulator design in SolidWorks and (b) a back trimetric view of the final AFO simulator design in SolidWorks.

Fabrication

The 3D printed parts are shown in Figure 15. The white parts were printed on an Ultimaker 3 Extended and the black parts were printed on an Ultimaker 5. All parts were printed with a 70% infill.

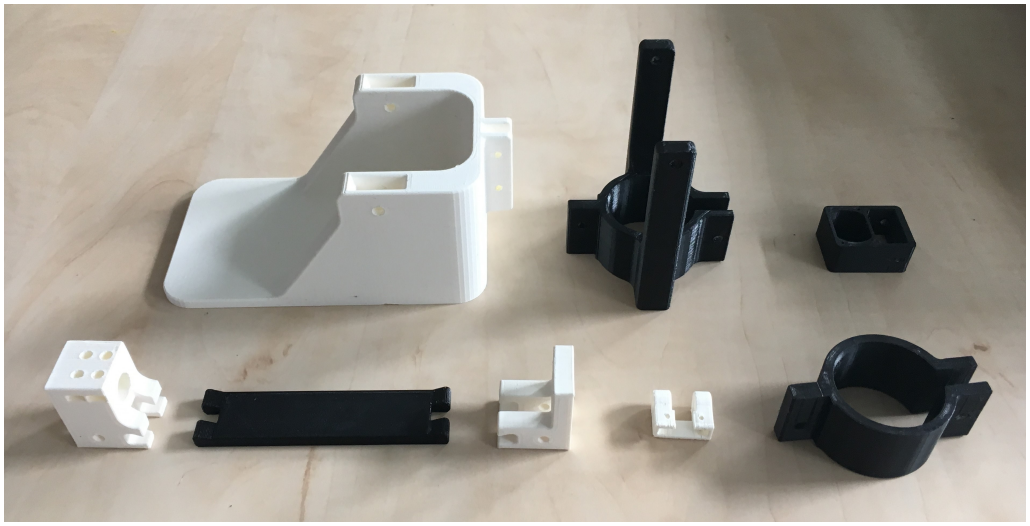

Figure 15: The individual 3D printed parts.

The parts shown in Figure 16 were ordered and then, if required, milled and/or turned in one of the workshops in the mechanical engineering faculty, 3mE, at the TU Delft. The cam ended up being CNC'd from a brass block, as its size was the most appropriate and readily available in the workshop. This was possible, as the hardness of brass is similar to that of steel.

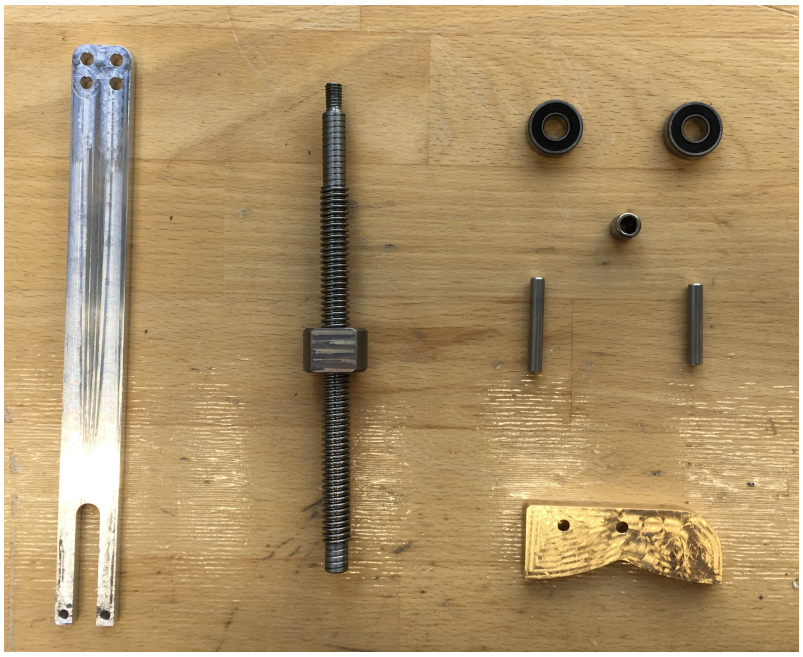

Figure 16: The post-processed and off-the-shelf parts of the AFO simulator.

Finally, the full assembly is shown in Figure 17 after each part was fabricated, adjusted and assembled.

Figure 17: Assembly AFO simulator version 1.

3 Experimental methods

In this section the experiment setup and data analysis are explained.

3.1 Equipment

In order to find out how well the proof-of-principle design works in reality, a dedicated AFO stiffness tester was used. The setup, a Bi-articular Reciprocal Universal Compliance Estimator (BRUCE), see Figure 18a, was used to measure the AFO simulator ankle stiffness at different slider positions. The design is based on a replicated human leg that is manually driven and continuously measures the joint angle and force exerted by the AFO onto the device. The force sensors are located in such a way that the moment of the AFO onto the device can be calculated, regardless of the point of force application on the device. The registered forces and joint configurations are transferred to a standard PC for further processing. The measured data are displayed real time in custom made software, based on MATLAB (The MathWorks, Natick, MA, USA). User feedback during operation is provided by plotting the measured angle versus the net moment.

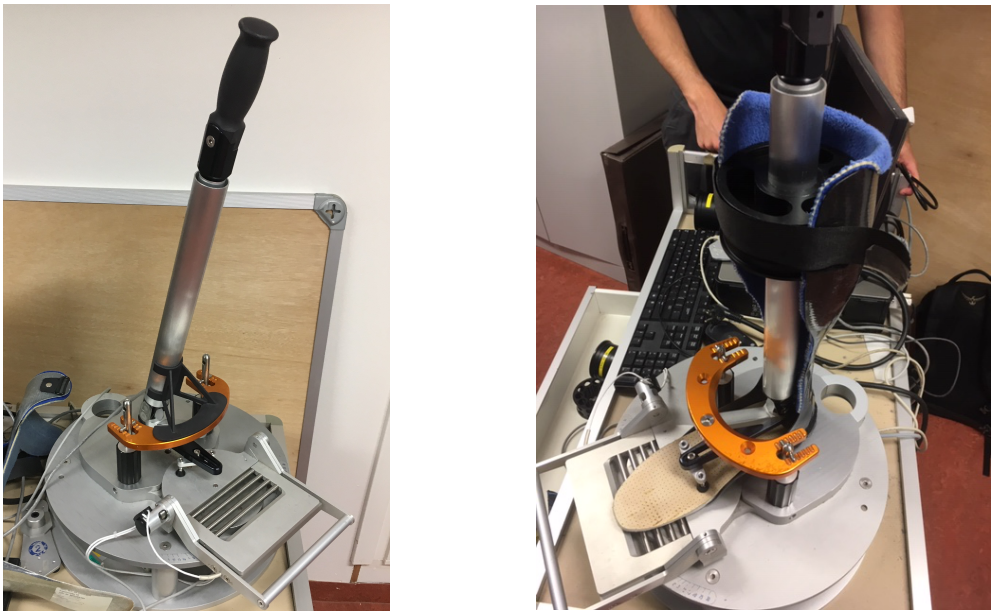

(a) (b)

Figure 18: (a) The BRUCE setup without AFO and (b) The BRUCE setup with an AFO.

3.2 Protocol

The AFO simulator was clamped to the 40mm tube of the BRUCE and its rotational axis was aligned with the rotational axis of the BRUCE, see Figure 19. Using a dummy foot, the rubber nuts on both sides of the ground plate and the orange C-shaped metal piece, the AFO simulator was clamped to the ground plate. To measure the ankle stiffness in both plantarflexion and dorsiflexion direction, the black handle at the top of the tube (representing the shank) could manually be moved both ways.

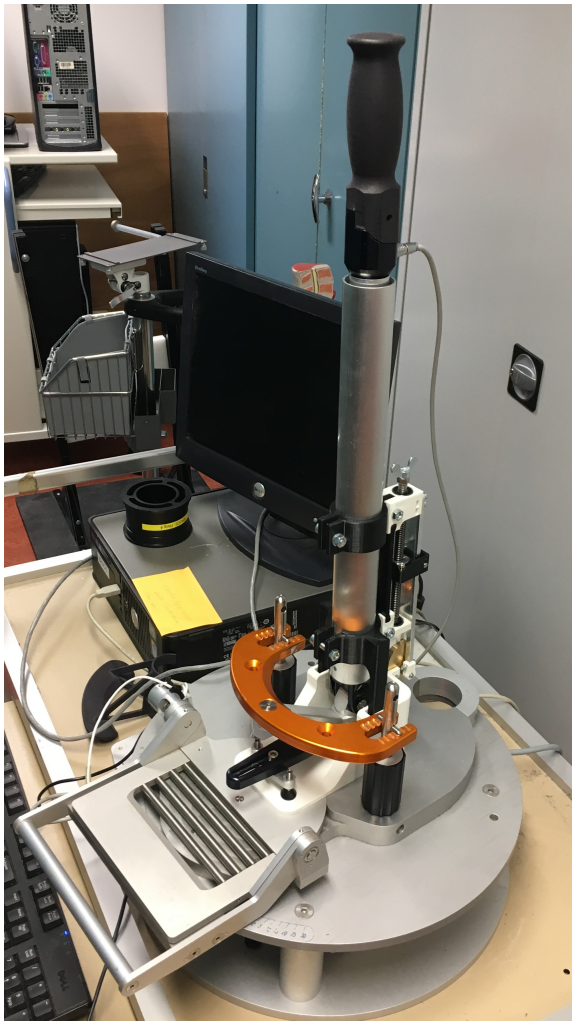

Figure 19: BRUCE with the AFO simulator.

The AFO simulator was moved into either maximum dorsiflexion or plantarflexion and slowly released towards the neutral angle, each repeated three times. The exerted external moment and the ankle angle were measured during this action. This was done three times for the first slider settings to test the consistency of the measurements. After the consistency was confirmed, the measurements were done two times instead of three for both dorsiflexion and plantarflexion at different slider positions. The range of torque-angle curves were experimentally determined by changing the slider position with increments of 10mm from the stiffest to the most compliant setting. Figure 20a and Figure 20b show how the leaf spring is deflected by the cam part.

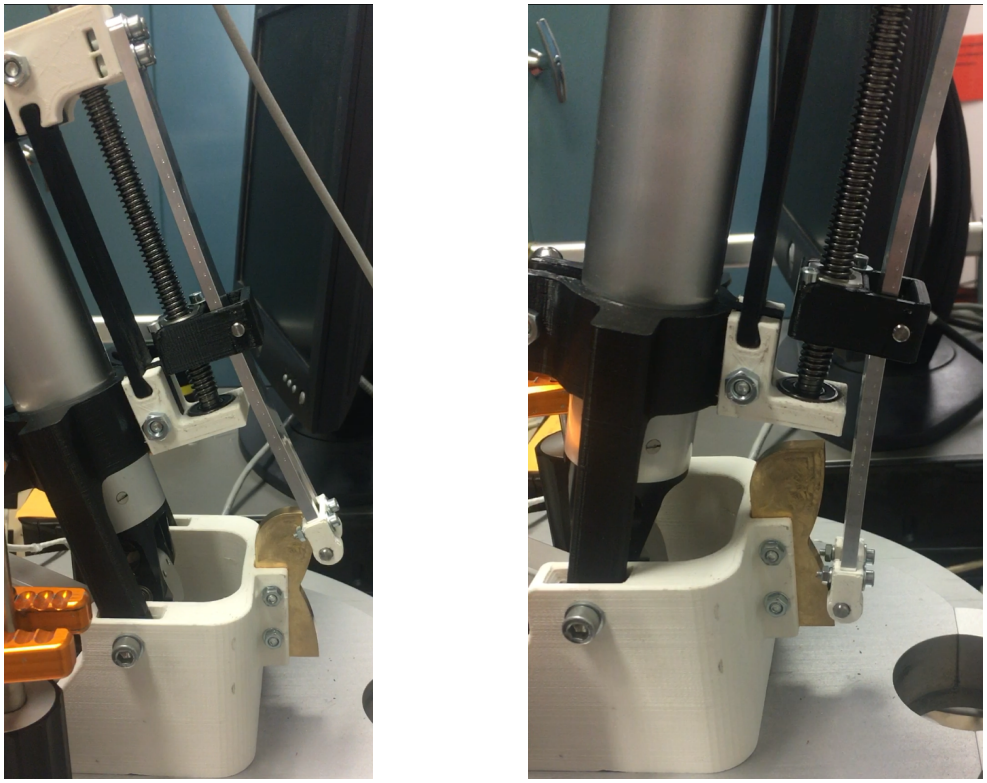

(a) (b)

Figure 20: (a) AFO simulator in a maximum dorsiflexed position and (b) in the maximum plantarflexed position

3.3 Data analysis

The torque-angle curves consisting of the measured data were plotted using a custom written MATLAB script. Over the AFO simulator linear stiffness phase, a linear fit was plotted, and the slope of this line was used to calculate the stiffness determined as: change in ankle moment divided by change in ankle angle.

4 Results

The custom MATLAB script used to monitor the benchtop testing of the AFO simulator, displayed plots as shown in Figure 21. To end up with the averaged stiffness, four points had to be chosen in that plot: Two points on the green line, representing the simulator ankle angle, on a positive slope and two points on the negative slope. The stiffness is then calculated by the custom MATLAB script with the following formula:

$$k = \frac{1}{2}\left(\frac{T_2 - T_1}{\theta_2 - \theta_1} + \frac{T_4 - T_3}{\theta_4 - \theta_3}\right) \tag{17}$$

With T being the torque at a certain simulator ankle angle θ and with k as the resulting averaged stiffness of the simulator.

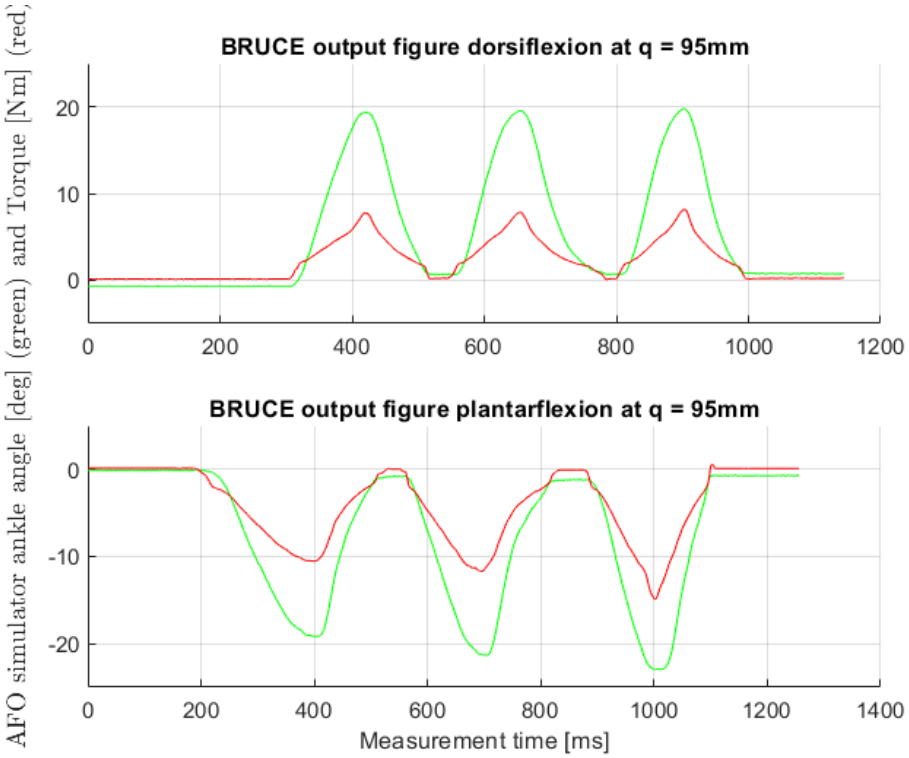

Figure 21: Two BRUCE output plots with the red line representing the torque and the green line representing the corresponding simulator ankle angle. Where q is the distance from the slider to the end of the leaf spring.

The experimentally determined ankle torque-angle curves at all slider positions are shown in Figure 22. The plantarflexion stiffness is 0.74 Nm/deg for the stiffest torque-angle curve, and 0.13 Nm/deg at the least stiff curve. For the dorsiflexion stiffness the maximum stiffness is 0.35 Nm/deg, and 0.07 Nm/deg at the least stiff curve. It can clearly be seen that the leaf spring had a certain pretension on the cam, as the dorsiflexion and plantarflexion torque-angle curves are connected by a relatively high stiffness curve. An increasing pretension of the leaf spring on the cam, would increase the amount of force that is needed to 'break free' from the neutral simulator ankle angle. Even though the pretension slightly increases the maximum stiffness in both directions, it does cause the AFO simulator to not have a perfect linear torque-angle curve as desired. Therefore,

ideally there should be zero pretension in the leaf spring. However, a small pretension is desired as to avoid backlash.

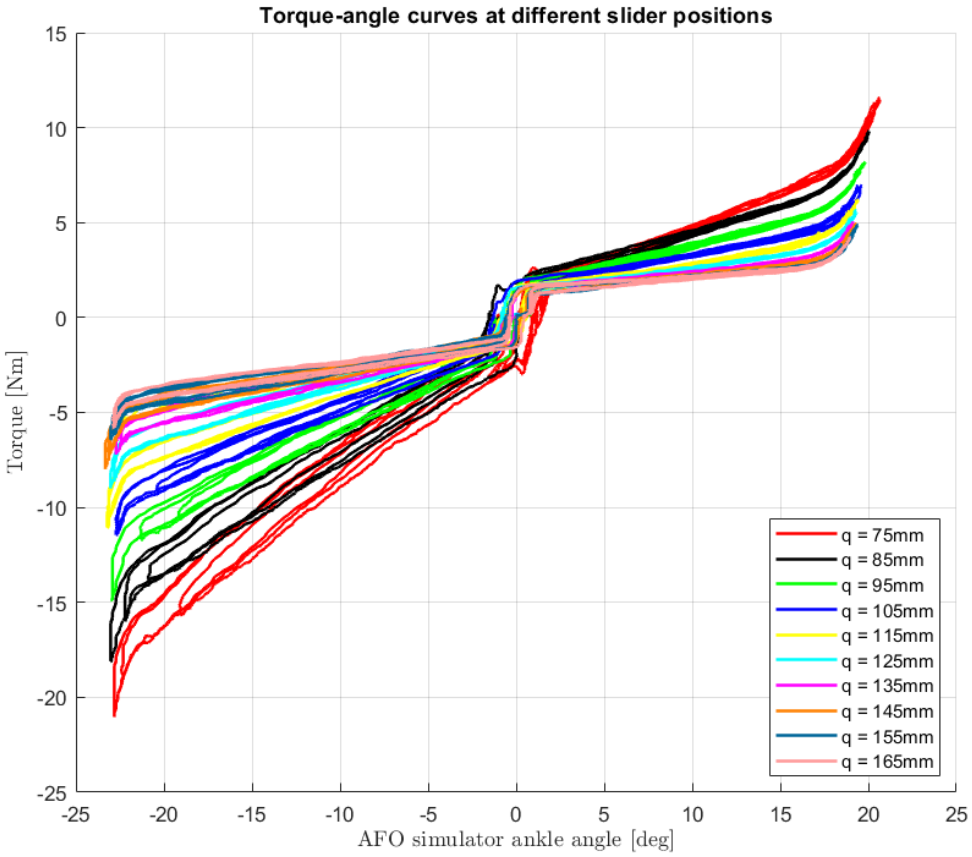

Figure 22: Torque-angle curves at all stiffness settings.

Furthermore, note the stiffness peaks at the end of both dorsiflexion and plantarflexion curves. These are caused by the simulator reaching the hard stops. Roughly an extra 3 degrees on both sides is reached when the simulator is pushed pass the hard stop and slightly starts bending. The ROM is approximately 43 degrees, which is 3 degrees higher than predicted. Looking at the two torque-angle curves at the maximum and minimum stiffness setting in Figure 23, more hysteresis occurs in the maximum stiffness setting than in the minimum stiffness setting in the plantarflexion range. In the dorsiflexion range hardly any hysteresis occurs.

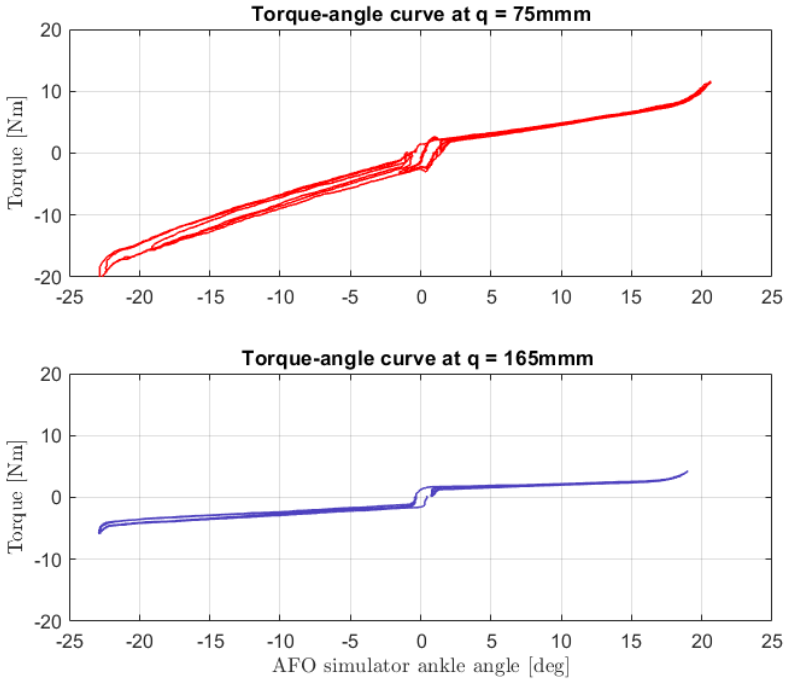

Figure 23: Two torque-angle curves

In Figure 24, the average measured dorsiflexion stiffness is plotted versus the mathematically predicted dorsiflexion stiffness. The measured stiffness values are roughly two times lower than the predicted stiffness values.

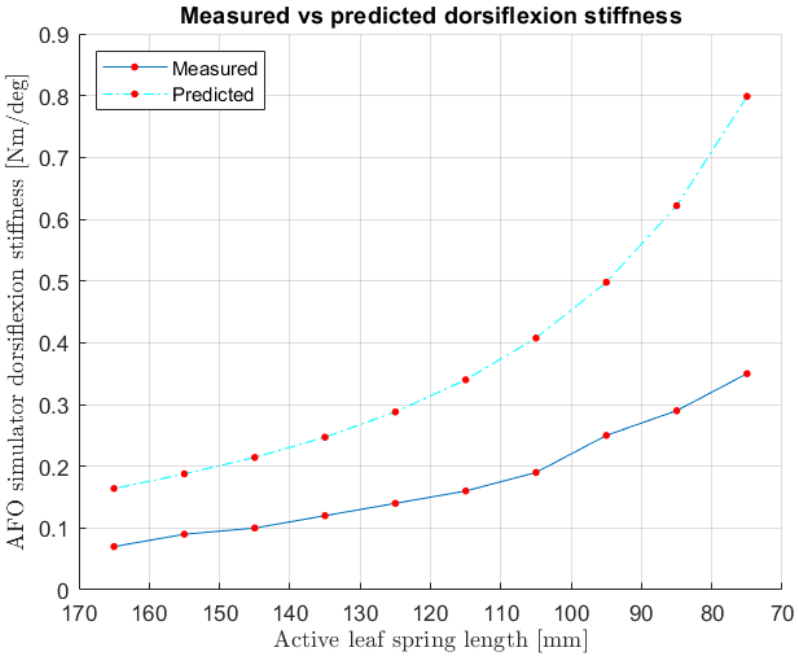

Figure 24: Measured vs predicted dorsiflexion stiffness.

In contrast to the measured dorsiflexion stiffness, the measured plantarflexion stiffness is on average only 0.035 Nm/deg lower than the predicted plantarflexion stiffness, see Figure 25.

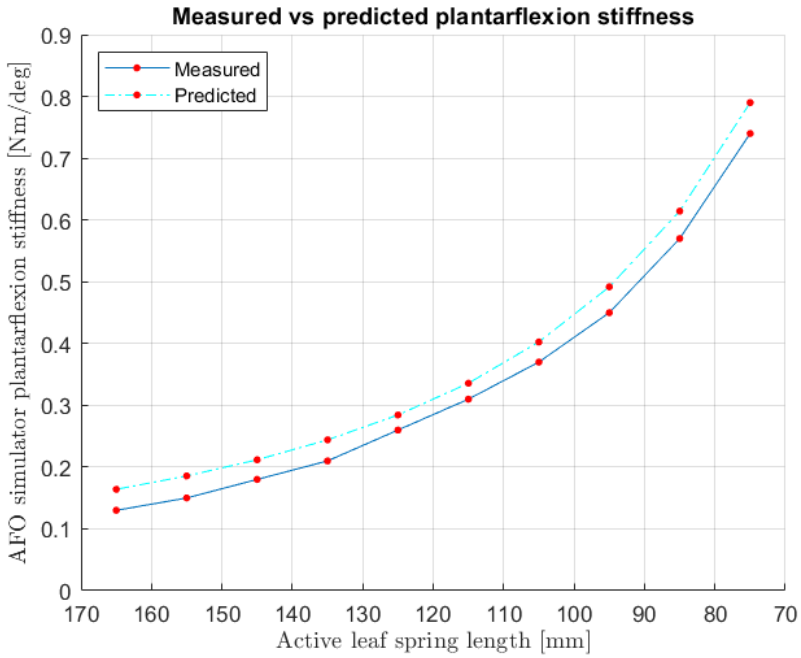

Figure 25: Measured vs predicted plantarflexion stiffness.

5 Discussion

In this report, the design and validation of an AFO simulator with continuously variable stiffness is described. The VSM can change the AFO simulator's stiffness, while being compact and lightweight. The goal for the VSM was to allow the realized AFO simulator to have a stiffness range similar to that of the predicted stiffness range. An offset is allowed, as long as the difference between the maximum and minimum stiffness is similar to the predicted stiffness range. A proof-of-principle of the AFO simulator was fabricated and then validated with a dedicated AFO stiffness tester (BRUCE) based on manual deflection of the AFO simulator. The tests showed promising results, but did not yet entirely show the desired behavior. In this section the results are discussed and are put into perspective.

The characterization of the AFO simulator showed that the ankle's torque-angle curve in plantarflexion direction closely matched the predicted torque-angle curve from the mathematical model. The measured plantarflexion stiffness at each slider position on average differed 0.035 Nm/deg from the predicted plantarflexion stiffness values. This difference could have been caused by the following: First, the script did not account for slight deformation of the 3D printed parts. Second, a slight deflection in the lead screw occurred. Even though the deflection was calculated to be smaller than a tenth of millimeter in the worst case, it still contributed to a slightly lower measured stiffness. Finally, in the mathematical model, the leaf spring was modelled as a spring without any holes or cavities, thus not taking the rectangle that was cut out at the end of the leaf spring, that avoids collision with the cam, into account.

Furthermore, the measured dorsiflexion stiffness at each slider position was roughly two times smaller than predicted. The difference between the plantarflexion and dorsiflexion stiffness could possibly be explained by the VSM being able to slightly rotate relative to the shank of the BRUCE. Moreover, the 3D printed parts might have deformed more when the AFO simulator was dorsiflexed compared to when it was plantarflexed.

Both the differences between the predicted and measured stiffness values and the measured plantar- and dorsiflexion stiffness values could be minimized by taking the following actions. First, either more of the same 3D printed material, or a stronger material should be used at the connection of the VSM to the clamps. This should decrease the amount of deformation that might have occurred during loading. Second, at both connections between the VSM and the clamps, an extra bolt could be used to decrease bearing stress, and thus also the local deformation of the material. Moreover, it would prevent rotation of the VSM base relative to the clamps. Third, a cavity should be made at the back and inside of the AFO simulator foot, so that the dummy foot can be placed a few millimeters further back. This will allow the ankle axis of the BRUCE to be perfectly aligned with the ankle axis of the AFO simulator. The pretension caused by misalignment can then be avoided. Finally, the clamps around the BRUCE shaft should be tightened more than during the first test to minimize rotation of the clamps relative to the BRUCE shank.

A new design iteration was made, carrying all four actions above, see Figure 26. The VSM base now consists of one part instead of three, is wider, stiffer and has two holes at the top and bottom to connect to the clamps. Again, tests were carried out using BRUCE at the VUmc. As expected the difference between the predicted and measured stiffness values was decreased, but the large difference between the measured plantarflexion stiffness and

the measured dorsiflexion stiffness was still present. Other possible explanations comprise of the following: In dorsiflexion direction the back of the foot of the AFO simulator has to resist a relatively high torque compared to the torque during plantarflexion due to the top part of the cam sticking out. A deformation due to bending of this back part could cause the leaf spring to have a decreased deflection, hence decrease the measured stiffness.

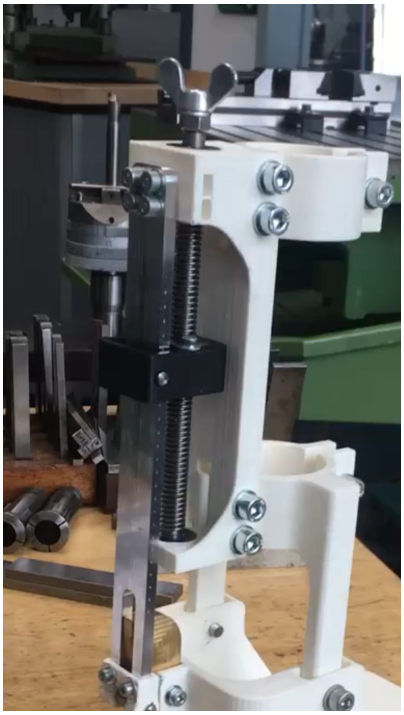

Figure 26: The improved VSM base.

Furthermore, in Figure 27, two free body diagrams of the VSM base are shown, one while the AFO simulator is plantarflexed and one while dorsiflexed. The resultant force F_{res} on the bottom part of the VSM can be calculated with $F_{res} = F_{S,bot} + F_{B,bot}$ when dorsiflexed in contrast to when the AFO simulator is plantarflexed, then $F_{res} = F_{S,bot} - F_{B,bot}$. Where $F_{B,bot}$ is the force from the BRUCE on the bottom of the VSM base and where $F_{S,bot}$ is the force from the lead screw on the VSM base. Hence, a relative larger deformation of this part occurs in dorsiflexion when compared to when the AFO simulator is plantarflexed. The deformation causes the pivot point of the leaf spring to move slightly away from the VSM base, resulting in a decreased deflection of the leaf spring.

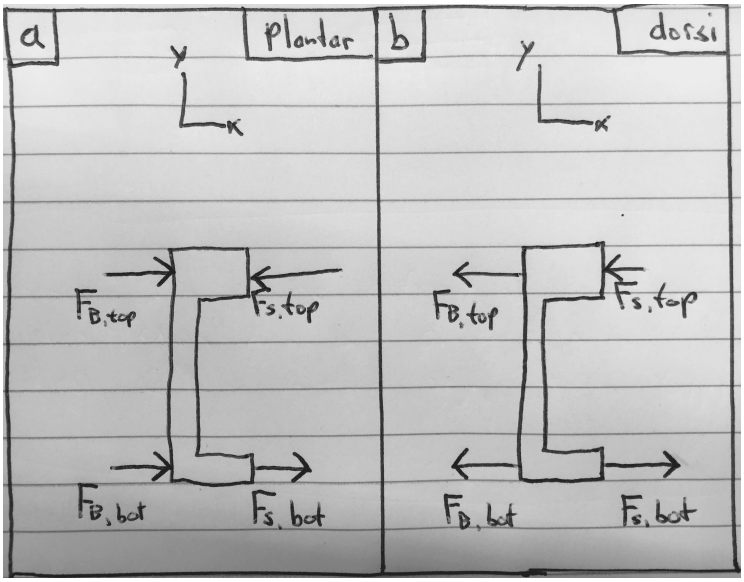

Figure 27: In sketch (a) a free body diagram is shown of the VSM base during plantarflexion and in sketch (b) during dorsiflexion.

When compared to literature [39], the plantarflexion stiffness range of the AFO simulator is comparable to AFOs of which the stiffness is changed discretely by changing its springs. A version could be made with a larger stiffness range, e.g. similar to that of the stiffness range of the dorsal-leaf-spring AFO used by Ploeger et al. [38], by using a stiffer leaf spring and a stronger VSM structure. This is further elaborated on in the future work chapter.

5.1 Limitations

It is important to note that the final design that will be worn by patients, will have to account for the following: Patients with spasticity in the dorsiflexor and/or plantar flexor muscles will put a constant stress on the AFO emulator, resulting in substantial higher torques required to change the slider position. It has become clear that the user group for the AFO simulator system will mostly consist of patients with some form of spasticity in their lower limb muscles. To ensure that the stiffness can still be modulated during gait even for patients with high levels of spasticity, a solution should be found for this problem. For example, by mounting a rail on the VSM to which the slider can be attached, resulting in reduced forces acting from the slider on the lead screw.

If the chosen VSM is used with a real AFO and tested by patients, the realizable stiffness range will be smaller due to attachment of the AFO simulator to the patient's leg. A human's lower limb soft tissues, such as skin, ligaments, tendons, and fat will cause an increased compliance between the AFO simulator and the patient's lower limb. The tighter the AFO simulator can be attached to the patient's leg, the better. However, an attachment that is too tight, will cause discomfort, so a trade-off must be made. Furthermore, the variability of joint center of rotation of a patient can cause misalignment in the joint's axes of the AFO simulator and the patient's ankle joint. As a result, the actual torque-angle curves can be different between subjects. To solve this, the researcher should do some static tests with the AFO simulator worn by the patient to find the actual torque-angle curves for each patient.

6 Conclusion

In this report, a design of an AFO simulator with continuously variable stiffness is introduced. The design process was described from start to end and the design was fabricated and tested. The VSM can change the stiffness of the AFO simulator, while being compact and lightweight. The linear torque-angle curve was created with a cam transmission, and the stiffness modulation was enabled by manual control of the leaf spring's support condition. The torque-angle curves were characterized for a cam profile that was made for level ground walking. One of the goals of the AFO simulator was to have a stiffness range similar to that of the predicted stiffness range. An offset was allowed, as long as the absolute value of the difference between the maximum and minimum stiffness was close to the predicted stiffness range. The AFO simulator was tested using BRUCE, a dedicated AFO stiffness tester. It was shown that the predicted plantarflexion stiffness range closely resembled the measured plantarflexion stiffness range, in contrast to the measured dorsiflexion stiffness range, which was roughly two times smaller than predicted.

6.1 Future work

The potential of the design has been presented, providing a next step for further development into a fully functional AFO simulator that can be worn by patients. Possible steps that are recommended to be taken in further studies are as follows: First, iterate on the current AFO simulator design until the desired stiffness range in both directions is found. Second, improve the design of the VSM so it is strong enough to reach a larger stiffness range. Then, design an AFO to which the VSM can be mounted to and that can be worn by patients. Third, replace the manual modulation of the slider position by electromechanical actuation. This could for example be done by putting a small actuator around the waist of the patient, and by transmitting the torque produced by this actuator through a flexible shaft to the lead screw. The clinician is then able to control the position of the slider from behind the computer, during the patient's gait. Finally, test and iterate on this design with patients and come to an usable device. This device could then help clinicians find the optimal stiffness of the orthoses they prescribe to specific patients in a time-efficient manner. An optimal stiffness could result in a more comfortable and less tiring gait, and therefore an increased quality of life for the patient.

References

[1] T. Oba, H. Kadone, M. Hassan, and K. Suzuki, "Robotic Ankle-Foot Orthosis with a Variable Viscosity Link Using MR Fluid," *IEEE/ASME Transactions on Mechatronics*, vol. 24, no. 2, pp. 495–504, 2019.

[2] B. S. Armour, E. A. Courtney-Long, M. H. Fox, H. Fredine, and A. Cahill, "Prevalence and causes of paralysis - United States, 2013," *American Journal of Public Health*, vol. 106, no. 10, pp. 1855–1857, 2016.

[3] M. J. Duncan, J. C. Spence, and W. K. Mummery, "Perceived environment and physical activity: A meta-analysis of selected environmental characteristics," *International Journal of Behavioral Nutrition and Physical Activity*, vol. 2, pp. 1–9, 2005.

[4] H. T. Hendricks, J. Van Limbeek, A. C. Geurts, and M. J. Zwarts, "Motor recovery after stroke: A systematic review of the literature," *Archives of Physical Medicine and Rehabilitation*, vol. 83, no. 11, pp. 1629–1637, 2002.

[5] M. Q. Liu, F. C. Anderson, M. G. Pandy, and S. L. Delp, "Muscles that support the body also modulate forward progression during walking," *Journal of Biomechanics*, vol. 39, no. 14, pp. 2623–2630, 2006.

[6] R. R. Neptune, S. A. Kautz, and F. E. Zajac, "Contributions of the individual ankle plantar flexors to support, forward progression and swing initiation during walking," *Journal of Biomechanics*, vol. 34, no. 11, pp. 1387–1398, 2001.

[7] A. Brashear, *Spasticity*. New York, NY: Springer Publishing Company, 12 2015.

[8] J. M. Perry, J.; Burnfield, "Gait Analysis, Normal and Pathological Function.," *The Journal of Bone & Joint Surgery*, vol. 75, no. 3, pp. 476–477, 1993.

[9] B. Chen, B. Zi, B. Chen, B. Zi, Y. Zeng, L. Qin, and W.-h. Liao, "Ankle-foot orthoses for rehabilitation and reducing metabolic cost of walking : Possibilities and challenges Mechatronics Ankle-foot orthoses for rehabilitation and reducing metabolic cost of walking : Possibilities and challenges ," *Mechatronics*, vol. 53, no. July, pp. 241–250, 2018.

[10] M. Alam, I. A. Choudhury, and A. B. Mamat, "Mechanism and design analysis of articulated ankle foot orthoses for drop-foot," *The Scientific World Journal*, vol. 2014, 2014.

[11] J. G. Pilitsis, "Spasticity – Causes, Symptoms and Treatments."

[12] C. L. Kuo and G. C. Hu, "Post-stroke Spasticity: A Review of Epidemiology, Pathophysiology, and Treatments," 12 2018.

[13] D. S. Roy and J. F. McLaughlin, "Spasticity," *Finnie's Handling the Young Child with Cerebral Palsy at Home*, pp. 367–374, 2009.

[14] ZonMw, "Richtlijn Beenorthesen," *Een klinisch handboek voor het verstrekken van beenorthesen naar maat bij mensen met blijvende ernstige zwakte of verlammingen van de beenspieren.*, vol. https://re, 2012.

[15] M. D. P. Webster, Joseph B., *Atlas of Orthoses and Assistive Devices*. 2019.

[16] Y. Jin, Y. He, and A. Shih, "Process Planning for the Fuse Deposition Modeling of Ankle-Foot-Orthoses," *Procedia CIRP*, vol. 42, pp. 760–765, 2016.

[17] R. K. Chen, Y.-a. Jin, J. Wensman, and A. Shih, "Additive manufacturing of custom orthoses and prostheses—A review," *Additive Manufacturing*, vol. 12, pp. 77–89, 2016.

[18] R. Chin, E. T. Hsiao-Wecksler, E. Loth, G. Kogler, S. D. Manwaring, S. N. Tyson, A. Shorter, and J. N. Gilmer, "A pneumatic power harvesting ankle-foot orthosis to prevent foot-drop," 2009.

[19] N. Ramstrand and S. Ramstrand, "AAOP state-of-the-science evidence report: The effect of ankle-foot orthoses on balance - A systematic review," *Journal of Prosthetics and Orthotics*, vol. 22, no. PROCEEDINGS, 2010.

[20] S. Yamamoto, S. Ibayashi, M. Fuchi, and T. Yasui, "Immediate-term effects of use of an ankle–foot orthosis with an oil damper on the gait of stroke patients when walking without the device," *Prosthetics and Orthotics International*, 2015.

[21] D. Ferris, G. Sawicki, and A. Domingo, "Powered Lower Limb Orthoses for Gait Rehabilitation," *Topics in Spinal Cord Injury Rehabilitation*, 2005.

[22] S. Galle, P. Malcolm, S. H. Collins, and D. De Clercq, "Reducing the metabolic cost of walking with an ankle exoskeleton: interaction between actuation timing and power," *Journal of NeuroEngineering and Rehabilitation*, vol. 14, p. 35, 4 2017.

[23] K. Z. Takahashi, M. D. Lewek, and G. S. Sawicki, "A neuromechanics-based powered ankle exoskeleton to assist walking post-stroke: A feasibility study," *Journal of NeuroEngineering and Rehabilitation*, vol. 12, p. 23, 2 2015.

[24] L. M. Mooney and H. M. Herr, "Biomechanical walking mechanisms underlying the metabolic reduction caused by an autonomous exoskeleton.," *Journal of neuroengineering and rehabilitation*, vol. 13, p. 4, 1 2016.

[25] W. Van Dijk, C. Meijneke, and H. Van Der Kooij, "Evaluation of the achilles ankle exoskeleton," *IEEE Transactions on Neural Systems and Rehabilitation Engineering*, vol. 25, pp. 151–160, 2 2017.

[26] K. A. Shorter, G. F. Kogler, E. Loth, W. K. Durfee, and E. T. Hsiao-Wecksler, "A portable powered ankle-foot orthosis for rehabilitation," *The Journal of Rehabilitation Research and Development*, vol. 48, no. 4, p. 459, 2011.

[27] T. Y. Chung, "Lower Limb Orthoses," in *Braddom's Rehabilitation Care: A Clinical Handbook*, pp. 75–84, Elsevier Inc., 2018.

[28] T. M. Kepple, K. L. Siegel, and S. J. Stanhope, "Relative contributions of the lower extremity joint moments to forward progression and support during gait," *Gait and Posture*, vol. 6, no. 1, pp. 1–8, 1997.

[29] I. Jonkers, C. Stewart, and A. Spaepen, "The complementary role of the plantarflexors, hamstrings and gluteus maximus in the control of stance limb stability during gait," *Gait and Posture*, vol. 17, no. 3, pp. 264–272, 2003.

[30] K. H. Lee and R. N. M. Johnston, "Effect of below-knee bracing on knee movement: biomechanical analysis.," *undefined*, 1974.

[31] J. F. Geboers, J. H. Van Tuijl, H. A. Seelen, and M. R. Drost, "Effect of immobilization on ankle dorsiflexion strength," *Scandinavian Journal of Rehabilitation Medicine*, vol. 32, no. 2, pp. 66–71, 2000.

[32] J. W. Hwang, S. K. Lee, J. S. Park, S. H. Ahn, K. J. Lee, and S. J. Lee, "The effects of ankle weight loading on the walking factors of adults without symptoms," *Journal of Exercise Rehabilitation*, vol. 13, pp. 425–429, 8 2017.

[33] J. F. Veneman, R. Kruidhof, E. E. Hekman, R. Ekkelenkamp, E. H. Van Asseldonk, and H. Van Der Kooij, "Design and evaluation of the LOPES exoskeleton robot for interactive gait rehabilitation," *IEEE Transactions on Neural Systems and Rehabilitation Engineering*, vol. 15, pp. 379–386, 9 2007.

[34] E. Russell Esposito, K. A. Schmidtbauer, and J. M. Wilken, "Experimental comparisons of passive and powered ankle-foot orthoses in individuals with limb reconstruction," *Journal of NeuroEngineering and Rehabilitation*, vol. 15, no. 1, pp. 1–10, 2018.

[35] M. B. Yandell, J. R. Tacca, and K. E. Zelik, "Design of a Low Profile, Unpowered Ankle Exoskeleton That Fits Under Clothes: Overcoming Practical Barriers to Widespread Societal Adoption," *IEEE Transactions on Neural Systems and Rehabilitation Engineering*, 2019.

[36] N. F. Waterval, F. Nollet, J. Harlaar, and M. A. Brehm, "Modifying ankle foot orthosis stiffness in patients with calf muscle weakness: Gait responses on group and individual level," *Journal of NeuroEngineering and Rehabilitation*, vol. 16, no. 1, pp. 1–9, 2019.

[37] D. J. J. Bregman, J. Harlaar, C. G. M. Meskers, and V. de Groot, "Spring-like Ankle Foot Orthoses reduce the energy cost of walking by taking over ankle work," *Gait & Posture*, vol. 35, no. 1, pp. 148–153, 2012.

[38] H. E. Ploeger, N. F. Waterval, F. Nollet, S. A. Bus, and M. A. Brehm, "Stiffness modification of two ankle-foot orthosis types to optimize gait in individuals with non-spastic calf muscle weakness-A proof-of-concept study," *Journal of Foot and Ankle Research*, vol. 12, no. 1, pp. 1–12, 2019.

[39] Y. L. Kerkum, A. I. Buizer, J. C. Van Den Noort, J. G. Becher, J. Harlaar, and M. A. Brehm, "The effects of varying ankle foot orthosis stiffness on gait in children with spastic cerebral palsy who walk with excessive knee flexion," *PLoS ONE*, vol. 10, no. 11, 2015.

[40] J. R. Koller, D. H. Gates, D. P. Ferris, and C. D. Remy, "Confidence in the curve: Establishing instantaneous cost mapping techniques using bilateral ankle exoskeletons," *Journal of Applied Physiology*, vol. 122, no. 2, pp. 242–252, 2017.

[41] D. Totah, M. Menon, C. Jones-Hershinow, K. Barton, and D. H. Gates, "The impact of ankle-foot orthosis stiffness on gait: A systematic literature review," *Gait and Posture*, vol. 69, no. October 2018, pp. 101–111, 2019.

[42] T. Kobayashi, M. L. Singer, M. S. Orendurff, F. Gao, W. K. Daly, and K. B. Foreman, "The effect of changing plantarflexion resistive moment of an articulated ankle-foot orthosis on ankle and knee joint angles and moments while walking in patients post stroke," *Clinical Biomechanics*, vol. 30, no. 8, pp. 775–780, 2015.

[43] B. Y. R. V. A. N. Ham, T. G. Sugar, B. Vanderborght, K. W. Hollander, and D. Lefeber, "Review of Actuators with Passive Adjustable Compliance/Controllable Stiffness for Robotic Applications," no. September, pp. 81–94, 2009.

[44] S. Wolf, G. Grioli, O. Eiberger, W. Friedl, M. Grebenstein, H. Hoppner, E. Burdet, D. G. Caldwell, R. Carloni, M. G. Catalano, D. Lefeber, S. Stramigioli, N. Tsagarakis, M. Van Damme, R. Van Ham, B. Vanderborght, L. C. Visser, A. Bicchi, and A. Albu-Schaffer, "Variable Stiffness Actuators: Review on Design and Components," *IEEE/ASME Transactions on Mechatronics*, vol. 21, no. 5, pp. 2418–2430, 2016.

[45] B. Vanderborght, A. Albu-Schaeffer, A. Bicchi, E. Burdet, D. G. Caldwell, R. Carloni, M. Catalano, O. Eiberger, W. Friedl, G. Ganesh, M. Garabini, M. Grebenstein, G. Grioli, S. Haddadin, H. Hoppner, A. Jafari, M. Laffranchi, D. Lefeber, F. Petit, S. Stramigioli, N. Tsagarakis, M. Van Damme, R. Van Ham, L. C. Visser, and S. Wolf, "Variable impedance actuators: A review," *Robotics and Autonomous Systems*, vol. 61, pp. 1601–1614, 12 2013.

[46] D. J. Braun, V. Chalvet, T. H. Chong, S. S. Apte, and N. Hogan, "Variable Stiffness Spring Actuators for Low-Energy-Cost Human Augmentation," *IEEE Transactions on Robotics*, vol. 35, no. 6, pp. 1435–1449, 2019.

[47] C. P. Chou and B. Hannaford, "Measurement and modeling of McKibben pneumatic artificial muscles," *IEEE Transactions on Robotics and Automation*, vol. 12, no. 1, pp. 90–102, 1996.

[48] B. Verrelst, R. Van Ham, B. Vanderborght, F. Daerden, D. Lefeber, and J. Vermeulen, "The pneumatic biped "lucy" actuated with pleated pneumatic artificial muscles," *Autonomous Robots*, vol. 18, pp. 201–213, 3 2005.

[49] K. W. Hollander, T. G. Sugar, and D. E. Herring, "Adjustable robotic tendon using a 'jack spring'™," in *Proceedings of the 2005 IEEE 9th International Conference on Rehabilitation Robotics*, vol. 2005, pp. 113–118, 2005.

[50] R. Van Ham, B. Vanderborght, M. Van Damme, B. Verrelst, and D. Lefeber, "MACCEPA, the mechanically adjustable compliance and controllable equilibrium position actuator: Design and implementation in a biped robot," *Robotics and Autonomous Systems*, vol. 55, pp. 761–768, 10 2007.

[51] S. Wolf and G. Hirzinger, "A new variable stiffness design: Matching requirements of the next robot generation," in *Proceedings - IEEE International Conference on Robotics and Automation*, pp. 1741–1746, 2008.

[52] M. D. C. Sanchez-Villamañan, J. Gonzalez-Vargas, D. Torricelli, J. C. Moreno, and J. L. Pons, "Compliant lower limb exoskeletons: A comprehensive review on mechanical design principles," 5 2019.

[53] S. Grosu, C. R. Guerrero, V. Grosu, B. Vanderborght, and D. Lefeber, "Evaluation and Analysis of Push-Pull Cable Actuation System Used for Powered Orthoses," vol. 5, no. September, pp. 1–11, 2018.

[54] S. Ferrier, M. Drielsma, G. Manion, and G. Watson, "Extended statistical approaches to modelling spatial pattern in biodiversity in northeast New South Wales. II. Community-level modelling," *Biodiversity and Conservation*, vol. 11, pp. 2309–2338, 12 2002.

[55] J. F. Veneman, R. Ekkelenkamp, R. Kruidhof, F. C. Van Der Helm, and H. Van Der Kooij, "A series elastic- and bowden-cable-based actuation system for use as torque actuator in exoskeleton-type robots," *International Journal of Robotics Research*, vol. 25, pp. 261–281, 3 2006.

[56] "Intelligent Robotics and Applications: Third International Conference, ICIRA ... - Google Boeken."

[57] J. W. Hurst, J. E. Chestnutt, and A. A. Rizzi, "An actuator with physically variable stiffness for highly dynamic legged locomotion," in *Proceedings - IEEE International Conference on Robotics and Automation*, vol. 2004, pp. 4662–4667, Institute of Electrical and Electronics Engineers Inc., 2004.

[58] M. A. LeBlanc, "Evaluation of Cable Vs. Hydraulic Transmission of Forces for Body-Powered Arm Prostheses.," pp. 71–73, 1985.

[59] M. K. Shepherd and E. J. Rouse, "Design of a quasi-passive ankle-foot prosthesis with biomimetic, variable stiffness," *Proceedings - IEEE International Conference on Robotics and Automation*, pp. 6672–6678, 2017.

[60] Machinedesign, "Flexible rotary shaft operation, uses, and advances — Machine Design."

[61] E. Barrett, M. Fumagalli, and R. Carloni, "Elastic energy storage in leaf springs for a lever-arm based variable stiffness actuator," *IEEE International Conference on Intelligent Robots and Systems*, vol. 2016-Novem, pp. 537–542, 2016.

[62] T. Letcher and M. Waytashek, "Material property testing of 3D-printed specimen in pla on an entry-level 3D printer," *ASME International Mechanical Engineering Congress and Exposition, Proceedings (IMECE)*, vol. 2A, no. February, 2014.

A Appendix A

Review on each subsystem

A.1 Variable stiffness mechanisms

To find possibilities regarding the VSM, I looked in the area of variable stiffness actuators. These systems closely resemble techniques that can be used to reach the goal of this project and are found in reviews in literature ([43], [44] and [45]).

A.1.1 Equilibrium-controlled stiffness

Series elastic actuator
Pros:

- High torque
- Highest accuracy for positioning
- Relatively small dimensions
- Relatively easy controllable
- Relatively quiet
- (Can include encoders to control velocity, position, torque and applied force)

Cons:

- Weight
- Mechanical impedance due to motor inertia and gears transmission (affects backdrivability)

A.1.2 Antagonistic-controlled stiffness

Two nonlinear springs (mechanisms)
Pros:

- Stiffness curve can be designed
- Similar to human joint stiffness

Cons:

- Limited stiffness range
- Might cause asymmetry
- Size
- Complexity
- Friction
- Energy costly to vary stiffness

Two PAMs
Pros:

- Muscle-like force length properties
- Intrinsic elasticity
- Lightweight
- High power/weight and power/volume ratio
- Back drivability
- Safe
- No stick or slip

Cons:

- Need pneumatic or hydraulic installation
- Nonlinear force-contraction (complex control)
- OK accuracy and repeatability
- Friction and compressibility of air
- Noise
- Pressure losses Extra:
- Cor from experience: pressure hard to control

Two hydro muscles
Pros:

- Lightweight
- High power/weight ratio
- High speeds
- Stability due to incompressibility of fluids

- Relatively few moving parts
- Overload protection
- Pumps and motors can be distant with minimal loss of power

Cons:

- Bulky system (Fluid reservoir, motors, pumps, release valves, heat exchangers and noise-reduction equipment)
- Expensive
- High-powered energy source required
- Leakage problem hard to solve
- Still in development stage Extra:
- Cor: need custom (expensive) parts for this application

Pully variations
Pros:

- Stiffness curve can be designed

Cons:

- Weight of two actuators
- Complex control
- Size
- Many parts
- Friction
- Both actuators have to be used to influence only one variable: compliance or equilibrium position.

A.1.3 Structure-controlled stiffness

Vary active spring length
Pros:

- Low force to change stiffness
- High stiffness range
- Lightweight

Cons:

- Limited range of motion

Vary cross section area
Pros:

- Simple construction

Cons:

- Only two predefined stiffness settings
- Lateral buckling Extra:
- Large stiffness range if many layered sheets are pressed together, but high force needed to hold sheets together as shear force is very high.

Vary elasticity modulus
Pros:

- Continuously variable stiffness

Cons:

- Only two predefined stiffness settings Can only be changed by changing temperature which takes too much time

A.1.4 Mechanically controlled stiffness

Change pretension (Vary lever arm length, MACCEPA and VS JOINT)
Pros:

- Linear angle-torque characteristic

Cons:

- Needs two actuators
- Weight
- Complex

Continuously variable transmission (Variable diameter pulley, Reeves drives and roller-based CVT)
Pros:

- Continuous variable stiffness
- Energy efficient
- Able to store negative work

Cons:

- Needs multiple actuators
- WeightWeight
- Complex
- Many parts

A.2 Other subsystems

A.2.1 Location variable stiffness mechanism

Onboard
Pros:

- No disadvantages of flexible transmission

Cons:

- Weight (depending on the chosen VSM)

Offboard
Pros:

- Powerful actuators possible
- AFO light weight
- Control loop bandwidths improved with desktop real-time controllers
- Faster iterations on the design, build and evaluation process (don't have to build a self-contained, untethered, batter-powered wearable device)
- Control changed through software instead of slow hardware design changes

Cons:

- Disadvantages of flexible transmission

A.2.2 Transmission

Bowden cable
Pros:

- Flexibility
- Relative long distance transmission
- Lightweight
- Often used
- Off-the-shelf

Cons:

- Stick and slack
- Hysteresis
- Friction

Push-pull cable
Pros:

- Can transfer force in two directions
- Only 1 instead of 2 cables
- Avoids asymmetry
- Robust

Cons:

- Weight

Tube (air and fluid)
Pros:

- 90% efficiency in all routing settings of hydraulic line
- High durability
- Offers good sensory feedback
- Can transmit push and pull forces

Cons:

- Need to have very precisely custom manufactured pistons
- Leaks
- Weight due to pistons

Comparison air vs fluid

- Require more volume for the same mechanical energy delivered
- Provide a "spring" coupling between master and slave
- Have a lag in its response to rapid actuation

- Make socially unacceptable noise when vented to the outside.

Rigid tube
Pros:

- No hysteresis, stick or slip
- Direct transmission

Cons:

- Not flexible
- Displacement of angle to high and not suitable for our problem.

Electrical wires
Pros:

- Less delay than wifi signal

Cons:

- Make sure wires are not in the way

Wireless
Pros:

- No wires in the way during walking

Cons:

- Slight delay

A.2.3 Stiffness adjustment

Actuator(s)
Pros:

- Allows researcher to have specific stiffness values for certain gait phases (like a semi-active AFO)
- Easily controlled from the computer

Cons:

- Extra (unnecessary) complexity at the start

Pull lever
Pros:

- Off-the-shelf can be self-locking
- Easy to apply required torque

Cons:

- Relative harder to change stiffness with small increments

Rotate screw
Pros:

- Is self-locking
- Can easily change stiffness by vary small increments

Cons:

- Takes relatively more time to change between extreme stiffness values

Winch
Pros:

- Easy to apply required torque
- 'Off-the-shelf'
- Small size

Cons:

- Self-locking in one way
- Not continuous stiffness setting anymore

B Appendix B

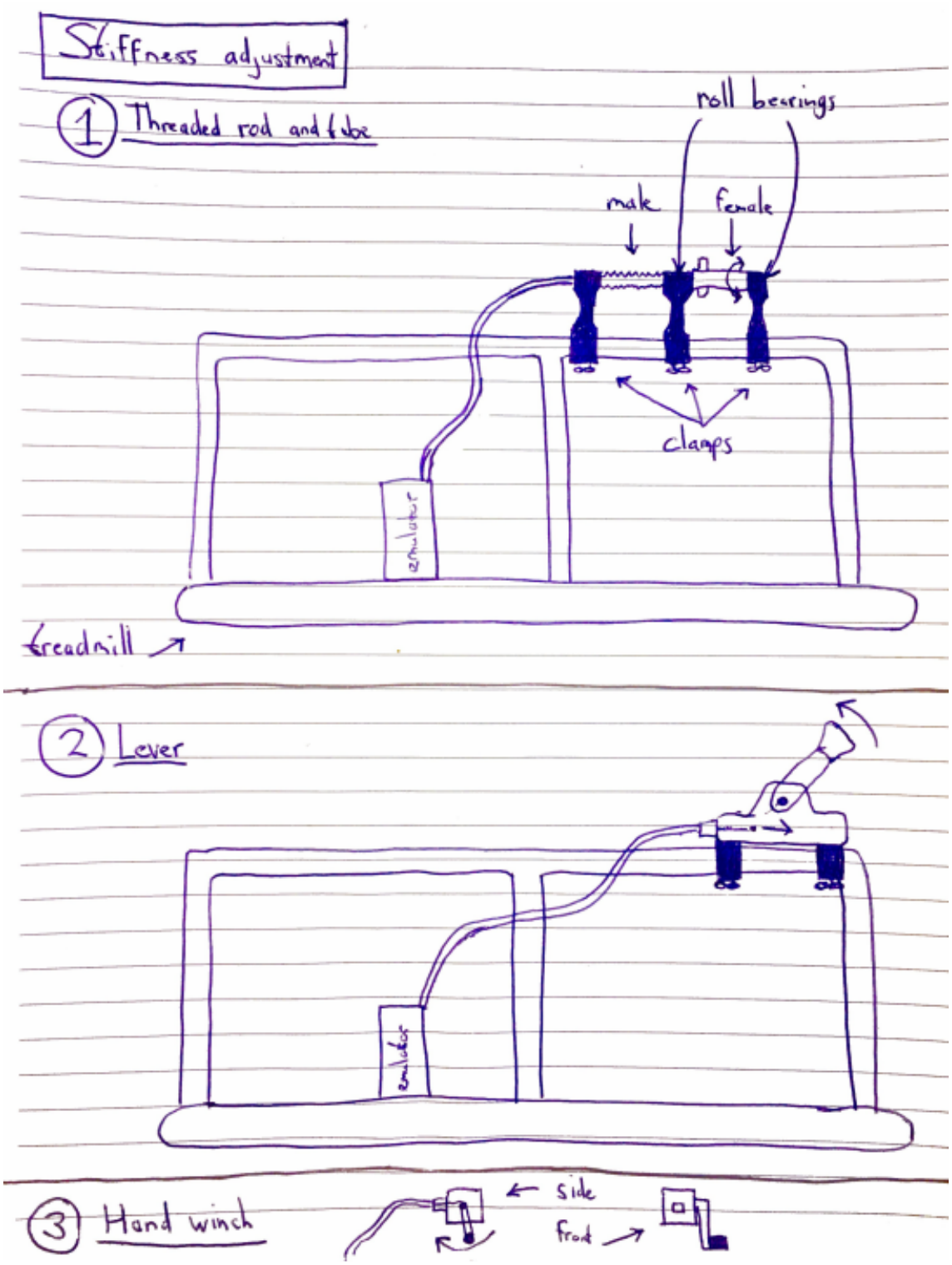

Figure 28: Sketch of stiffness adjustment mechanisms.

Subsystem	**Options**									
	Equilibrium-controlled stiffness	*Antagonistic-controlled stiffness*				*Structure-controlled stiffness*			*Mechanically controlled stiffness*	
VSM*	SEA**	Two nonlinear springs	Two Pneumatic Artificial Muscles	Two Hydro Muscles	Pulley variations	Vary active spring length	Vary cross section area	Vary elasticity modulus	Change pretension	CVM***
Location VSM	Onboard	Offboard								
Transmission	Bowden cable	Push-pull cable	Tube (air)	Tube (fluid)	Rigid tubes	Electrical wires	Wireless			
Stiffness adjustment	Actuator(s)	Pull lever	Rotate screw	Winch	Other					
Foot segment	Foot plate	Simplified foot plate								
Shank segment	Anterior	Posterior	Around top of shank	Simplified shank						

Figure 29: Morphological overview